UNIVERSITETET I AGDER

Energy analysis of cooling tower and metal holding tanks at Chassix

John-Are Sørlie

SUPERVISOR

Souman Rudra

University of Agder, [2018]

Faculty of Engineering and Science

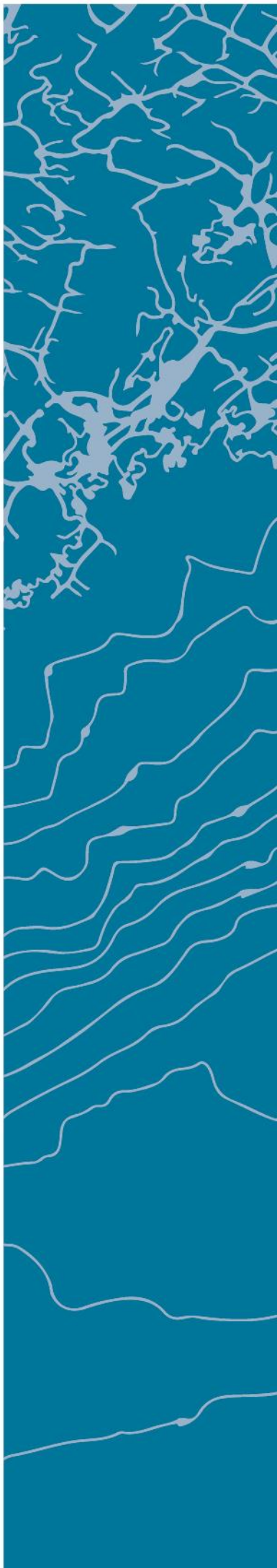

Abstract

In this thesis, two different methods were used attempting to estimate heat loss from metal holding tanks and chutes at Chassix Norway. The first method uses thermal resistance to calculate the total heat loss without any measurements, while the second calculates the conductive, convective and radiative heat loss separately using surface temperature measurements. Resulting heat loss for one year was 605.65 *MWh* without measurements and 827.64 *MWh* after surface temperature measurements. Heat loss calculated using measurements is the most accurate, as it relies on fewer assumptions.

Additionally, a model was created in Aspen Plus with basis in a cooling tower at Chassix, attempting to analyze the operations of the cooling tower using the distillation column block RadFrac. The process of finding the VLE (Vapor Liquid Equilibrium) diagram for water and air was presented, with the intention of using the McCabe-Thiele method to find the number of equilibrium stages suitable for the model. However, the VLE diagram proved unreasonable to use in the McCabe-Thiele method. The model was therefore run with a reasonable amount of equilibrium stages, based on an example model. This did not yield any useful results and it was clear the model did not run as intended. Despite this, simulating and analyzing a cooling tower in Aspen Plus should be possible as it has been done before, albeit with a more complex method.

Preface

This master thesis has been written as part of the graduation requirements for the master´s programme "Renewable Energy" at the University of Agder. The work on this thesis took place between January to June of 2018 and includes parts of the work from a research project serving as a prelude to this thesis.

The thesis was written in collaboration with Chassix Norway, who first submitted the thesis to the university. I chose this topic for my master thesis because I find energy analysis to be an interesting and engaging field of study with practical applications, especially in areas of industry. The research has been challenging and difficult, but the knowledge and experience I have gained is well worth the effort.

I would like to extend my thanks to my supervisor, Souman Rudra, whose guidance and advise has been invaluable. Additionally, Harry Danielsen and Sverre Gardøl, employees at Chassix, have provided useful information and hospitality during visits to Chassix.

Finally, my colleagues Kjartan Topstad Kondradsen and Endre Danielsen have supplied me with motivation and helpful discussions throughout the work.

I hope you enjoy reading

John-Are Sørlie

Grimstad, June 1, 2018

Individual/group Mandatory Declaration

The individual student or group of students is responsible for the use of legal tools, guidelines for using these and rules on source usage. The statement will make the students aware of their responsibilities and the consequences of cheating. Missing statement does not release students from their responsibility.

1.	I/We hereby declare that my/our thesis is my/our own work and that I/We have not used any other sources or have received any other help than mentioned in the thesis.	☒
2.	I/we further declare that this thesis: - has not been used for another exam at another department/university/university college in Norway or abroad; - does not refer to the work of others without it being stated; - does not refer to own previous work without it being stated; - have all the references given in the literature list; - is not a copy, duplicate or copy of another's work or manuscript.	☒
3.	I/we am/are aware that violation of the above is regarded as cheating and may result in cancellation of exams and exclusion from universities and colleges in Norway, see Universitets- og høgskoleloven §§4-7 og 4-8 og Forskrift om eksamen §§ 31.	☒
4.	I/we am/are aware that all submitted theses may be checked for plagiarism.	☒
5.	I/we am/are aware that the University of Agder will deal with all cases where there is suspicion of cheating according to the university's guidelines for dealing with cases of cheating.	☒
6.	I/we have incorporated the rules and guidelines in the use of sources and references on the library's web pages.	☒

Publishing Agreement

Authorization for electronic publishing of the thesis.

Author(s) have copyrights of the thesis. This means, among other things, the exclusive right to make the work available to the general public (Åndsverkloven. §2).

All theses that fulfill the criteria will be registered and published in Brage Aura and on UiA's web pages with author's approval.

Theses that are not public or are confidential will not be published.

I hereby give the University of Agder a free right to

make the task available for electronic publishing: ☒JA ☐NEI

Is the thesis confidential? ☐JA ☒NEI

(confidential agreement must be completed)

- If yes:

Can the thesis be published when the confidentiality period is over? ☐JA ☐NEI

Is the task except for public disclosure? ☐JA ☒NEI

(contains confidential information. see Offl. §13/Fvl. §13)

Table of Contents

List of Figures

List of tables

Nomenclature

A	Area [m^2]
A_n	Constant [-]
b	Constant [-]
B_n	Constant [-]
C_n	Constant [-]
D	Distillate to feed ratio [-]
f_d	Distillate flow [m^3/h]
f_f	Feed flow [m^3/h]
f_o	Bottoms [m^3/h]
f_p	Flow of top product removed [m^3/h]
f_r	Flow returned as reflux [m^3/h]
f_u	Boilup [m^3/h]
g	Standard gravity [m/s^2]
Gr_x	Grashof number [-]
h	Heat transfer coefficient [W/m^2*K]
k	Thermal conductivity [W/m*K]
L	Length/thickness of medium [m]
n	Amount of gas [mol]
N_e	Equilibrium stages [-]
N_p	Number of plates [-]
Nu_L	Nusselt number [-]
P_v	Vapor pressure [mmHg]
P	Pressure [Pa]
p_A	Partial vapor pressure of component A [atm]
P_A^0	Vapor pressure of pure component A [atm]
P_a^0	Vapor pressure of pure air [atm]
p_B	Partial vapor pressure of component B [atm]
P_B^0	Vapor pressure of pure component B [atm]
Pr	Prandtl number [-]
p_{tot}	Total vapor pressure [atm]
P_w^0	Vapor pressure of pure water [atm]

Q	Heat transfer [W]
Q_e	Rate of heat transfer by radiation [W]
Q_{cond}	Rate of heat transfer from direct contact [W]
Q_{conv}	Rate of heat transfer from area to fluid [W]
R	Gas constant= 8.314 [J/K*mol]
Ra_x	Rayleigh number [-]
R_{total}	Total thermal resistance in all layers [K/W]
R_{conv}	Thermal convective resistance [K/W]
R_f	Reflux ratio [-]
T_2	Temperature [K]
T_e	Ambient temperature [K]
T_f	Temperature of adjacent fluid [K]
T_i	Temperature on hot side [K]
T_j	Temperature on cold side [K]
T_s	Surface temperature [K]
T_{surr}	Temperature of surrounding area [K]
T_r	Reference temperature [K]
ΔT	Difference of surface and ambient temperature [K]
v	Kinematic viscosity [m^2/s]
V	Volume [m^3]
v_a	Vapor mole fraction of air [-]
V_B	Boilup ratio [-]
v_w	Vapor mole fraction of water [-]
x	Length [m]
x_a	Liquid mole fraction of air [-]
x_A	Liquid mole fraction of component A [-]
x_B	Liquid mole fraction of component B [-]
X_D	Distillate composition [-]
x_w	Liquid mole fraction of water [-]
x_b	Mole fraction of benzene [-]
α	Constant= 0,5 [-]

β Volumetric coefficient of expansion [K^{-1}]

ε Emissivity [-]

σ Stefan-Boltzmann constant = 5.67*10^{-8} [W/m^2*K^4]

η_p Plate efficiency [-]

1. Introduction

Cooling towers are common industrial devices used in the cooling of production, ventilation and other systems. They exploit the cooling effect that occurs when water evaporates and enhance it with forced or natural draft. The efficiency of cooling towers can have a substantial impact on energy consumption, and is consequently widely explored in regards to mathematical models that can predict their performance [1]. According to Jin et al [1] Merkel was the first to introduce a model to describe the operation of a cooling tower in 1925. Since then, several new, accurate methods have been proposed, among them the effectiveness-NTU method and Stoecker´s [2] empirical model based on polynomial approximation.

However, very little work has been done to explore the modeling of cooling towers in the program Aspen Plus. The only work belongs to Queiroz et al [3], who proposed an approach to simulate cooling tower performance by using Murphree efficiency and equilibrium stages to describe the operation. These parameters were optimized using the Levenberg-Marquardt method in Microsoft Excel, which was then integrated with Aspen Plus.

Considering this information, part of this thesis will focus on attempting to model a cooling tower of a commercial plant in Aspen Plus using another method. The VLE is applied to calculate the number of equilibrium stages necessary for the cooling tower simulation using the McCabe-Thiele method. Since the model block used in Aspen Plus, RadFrac, represents a distillation column, this method can be used while regarding the air and water that mixes in a cooling tower as two components to be separated in a distillation column.

Several areas in industry are interesting when referring to energy efficiency. Norway produces a lot of electricity from wind energy and hydropower [4], which is used in a variety of energy-intensive industries all over the country. The amount of electricity used by the energy-intensive industry in 2016 was 36.5 TWh, which is approximately 30 % of the total electricity produced, 122.4 *TWh* [4]. Chassix is part of this energy demanding sector, which has a substantial potential for reducing the energy consumption when improving energy efficiency. Optimizing the operations of a cooling tower could have a significant impact on consumption in the plant.

This thesis will also look at the energy consumption of electrical heating elements employed at Chassix to keep aluminum at a constant temperature of approximately 730 °C in liquid state within tanks and chutes. Keeping aluminum at this temperature requires significant amounts of energy and variations in insulation or other parameters has the potential to influence electricity consumption greatly. The heat loss will first be estimated based on calculations without measuring surface temperatures using thermal resistance, and then after measurements are taken. The results will then be compared to assess whether the calculations done before or after measurements are more accurate.

Finally, a Sankey diagram describing the total energy flow which has been estimated will be presented as a reference point to the results from the heat loss calculations, and where the energy analysis of the cooling tower would have fit in.

1.2 Background

Chassix is located in Farsund, Norway. The factory produces aluminum castings for the automotive market, with customers such as BMW, Ferrari and Rolls Royce. The aluminum used in their production is delivered in liquid form from Alcoa, just 200 *m* from the gate to Chassix.

In 2016, the electricity consumption of Chassix was 24119 *MWh*. With a total electricity cost of 0,40 *NOK/kWh*, this resulted in 9 647 600 *NOK* spent on electricity in 2016. Additionally, 3 *GWh* of energy is consumed in the form of propane each year for the sand mold production.

With such a substantial consumption, there is a strong motivation to map the flow of energy throughout the factory and identify where the energy losses are highest. Subsequently, this leads to awareness of what areas have the most potential for reduction in energy consumption.

1.3 Research questions

How much heat loss from the aluminum heating will be estimated using thermal resistance without any measurements, compared to calculations done after measuring the surface temperatures?

Is it possible to create a VLE diagram of an air-water mixture, and use that knowledge to find equilibrium stages for the cooling tower at Chassix?

Can the cooling tower be simulated in Aspen Plus when there are few previous examples of it?

1.4 Research limitations

During the work on this thesis, several factors presented difficulties. The original title for the thesis was vague, and it was necessary to modify it before the research could focus on relevant areas. Providing energy analysis for all areas in the production process at Chassix would have caused the workload to exceed the scope of this thesis.

New investments and projects at Chassix caused limitations on how much time and resources they could spare for this thesis. This caused the flow of information to be slower than it could have been, imposing some restrictions on how fast the thesis was progressing.

Finally, Aspen Plus was the only relevant program available for modeling and simulating in this thesis. It is mainly a tool for simulating and analyzing chemical processes. Consequently, aligning the options in Aspen Plus with a suitable title and appropriate research questions proved time-consuming, and a process with significant research and trial and error. On top of this, it was necessary to learn the program before these options could be explored.

2. Theory

2.1 Heat transfer

This chapter will present the three components heat loss comprises of, conduction, convection and radiation, as well as heat loss calculation by thermal resistance. Parts of this sub-chapter refers to earlier work in a research project [5].

2.1.1 Conduction

Conduction is the transfer of heat through a medium, which can be gas, solid or liquid. The rate of heat transfer is determined by the medium conductivity, medium thickness and temperature difference. Heat transfer is given by *Fourier´s law [6]*:

$$Q_{cond} = kA\left(\frac{T_2 - T_1}{L}\right) \quad (1)$$

where

Q_{cond} = Rate of heat transfer from direct contact [W]

k = Thermal conductivity [W/m*K]

A = Area [m^2]

T_2 = Temperature [K]

L = Length/thickness of medium [m]

An example of heat transfer by conduction is through a door in a house, where T_2 is the temperature inside, which is higher than T_1, the temperature outside. This gives a positive number in the x-direction, inside to outside.

2.1.2 Convection

Heat transfer from a solid surface to an adjacent liquid or gas is known as convection and happens as a combination of conduction and the bulk motion of gas or liquid. The movement of air around a radiator caused by the heating is an example of convection. The rate of heat transfer through convection is given by *Newton´s law of cooling [6]*:

$$Q_{conv} = hA(T_s - T_f) \quad (2)$$

where

Q_{conv} = Rate of heat transfer from area to fluid [W]

h = Heat transfer coefficient [W/m^2*K]

T_s = Surface temperature [K]

T_f = Temperature of adjacent fluid [K]

Convection resistance is useful when calculating a network of resistances through several layers [7]:

$$R_{conv} = \frac{1}{hA} \quad (3)$$

where

R_{conv} = Thermal resistance [K/W]

When energy is being transferred from a surface by convection, the motion of air can either be free-flowing or forced. Free-flowing means only the natural draft induced by the rising of hot air moves the air, while forced convection uses fans or motors to increase the rate of heat transfer. Forced convection typically increases rate of heat transfer by up to 10 times for gases, and up to 20 times for liquids [6].

Heat transfer coefficient of air with natural convection varies between 6 and 30 W/m^2*K [8]. This greatly affects the resulting heat transfer from convection, as it is directly proportional according to eq. (2). Finding the correct coefficient is therefore a critical step in finding the most accurate convective heat transfer. Mills [9] claims natural convection, such as heat rising from a heated wall, does not exceed a velocity of 2 *m/s*, and a typical value for gases is 5 W/m^2*K. To find the heat transfer coefficient of the tanks and chutes, heat flow on a vertical wall is considered. For this purpose, several steps have to be taken. First, the Rayleigh number for flow is needed. It is given by [9]:

$$Ra_x = \frac{\beta \Delta T g x^3}{v\alpha} \quad (4)$$

Where

Ra_x = Rayleigh number [-]

β = Volumetric coefficient of expansion [K^{-1}]

ΔT = Difference of surface and ambient temperature [K]

g = Gravitational constant [m/s^2]

x = Length [m]

v = Kinematic viscosity [m^2/s]

It can also be expressed as [9]:

$$Ra_x = Gr_x Pr \quad (5)$$

where

Gr_x = Grashof number [-]

Pr = Prandtl number [-]

Volumetric coefficient of gas [9]:

$$\beta = \frac{1}{T_r} \quad (6)$$

Mean film temperature, or reference temperature, is the mean of the surface and stream temperature. For external flows, the following equation defines the reference temperature used for calculations [9]:

$$T_r = T_s - \alpha(T_s - T_e) \quad (7)$$

Where

T_r = Reference temperature [K]

α = Constant= 0,5 [-]

T_e = Ambient temperature [K]

The Grashof number is defined as [9]:

$$Gr_x = \frac{\beta \Delta T g x^3}{v^2} \quad (8)$$

The Prandtl number varies with temperature. For air, however, it deviates only slightly from 0.69 for even high temperatures [9].

A function is defined based on the Prandtl number [9]:

$$\Psi = \left[1 + \left(\frac{0{,}492}{Pr}\right)^{\frac{9}{16}}\right]^{-\frac{16}{9}} \quad (9)$$

A function called the Nusselt number is then defined for laminar flow when $Ra_x \leq 10^9$ [9]:

$$Nu_L = 0{,}68 + 0{,}670(Ra_L \Psi)^{\frac{1}{4}} \quad (10)$$

Where

Nu_L = Nusselt number

The heat transfer coefficient can then be calculated from:

$$h = \frac{k}{L} Nu_L \quad (11)$$

2.1.3 Thermal Radiation

Thermal radiation is transferred by electromagnetic waves, unlike conduction and convection. It requires no adjacent medium to transfer heat, as electromagnetic waves can travel through vacuum. All objects emit thermal radiation, and the rate of heat emission is given by the *Stefan-Boltzmann law* [6]:

$$Q_e = \varepsilon \sigma A (T_s^4 - T_{surr}^4) \quad (12)$$

where

Q_e = Rate of heat transfer by radiation [W]

ε = Emissivity [-]

σ = Stefan-Boltzmann constant = $5.67*10^{-8}$ [W/m^2*K^4]

T_{surr} = Temperature of surrounding area [K]

Emissivity varies significantly for different types of steel, which is the surface material for the metal holding tanks and chutes at Chassix. Normal steel has more than 10 times lower emissivity than stainless steel [10].

2.1.4 Multilayer plane walls

To calculate heat transfer through a wall of multiple layers with different thermal resistance, consider Figure 1. This can be described as a *composite wall*, where thermal resistance in each layer is described as [7]:

$$R = \frac{x}{kA} \tag{13}$$

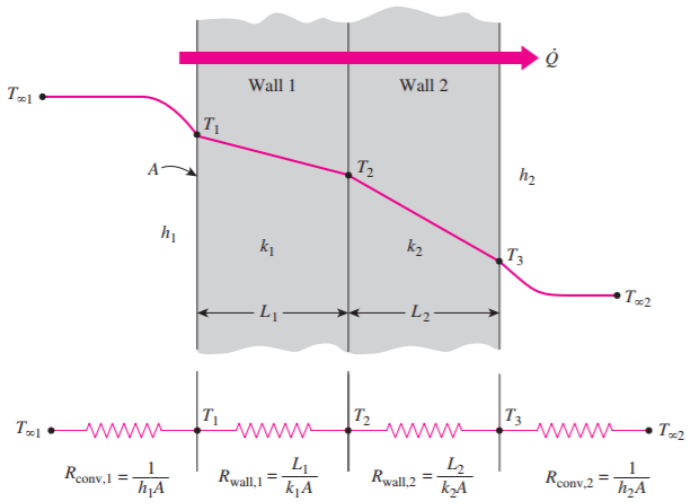

Figure 1: Two-layer wall[7].

Heat transfer from one side of a multilayered wall can be determined from the following equation [7]:

$$Q = \frac{T_i - T_j}{R_{total}} \tag{14}$$

where

Q = Heat transfer [W]

T_i = Temperature on hot side [K]

T_j = Temperature on cold side [K]

R_{total} = Total thermal resistance in all layers [K/W]

These multi-layer equations are based on the assumption that temperature increases or decreases through a single layer linearly.

2.2 Distillation column

A Distillation column is based on the principle of how different components of a mixture will have different boiling points. The vapor will contain more of the lower boiling point component, while the liquid has a higher concentration of the higher boiling point component [11].

Figure 2 illustrates the principles of a distillation column´s operation. A feed stream, consisting of two or more components, is fed into the column at middle height. Columns are divided into a certain number of “stages”, which indicates how many total trays or plates there are. If the number of stages

in a column is 10, the feed stream will typically enter at stage five [12]. The purpose of trays in the column is to increase the rate at which the feed stream is separated into its components, and are divided into several types, such as bubble cap, valve and sieve [11].

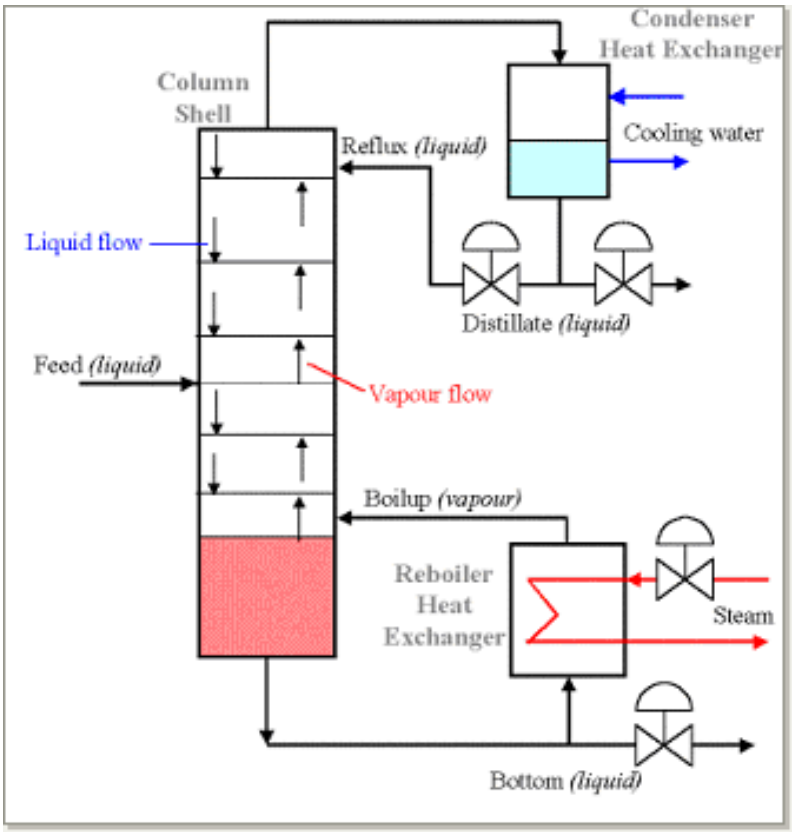

Figure 2: Distillation column principles [12].

In addition to trays, columns include a condenser and reboiler to increase the separation. Liquid that collects at the bottom of the column is sent to the reboiler, where heat is used to generate vapor, which travels back into the column. At the top, on the other hand, vapor is sent to a condenser supplied with cooling water, which condenses the vapor into liquid. At both the condenser and reboiler parts of the distillation column liquid is removed from the circulation as top or bottom product [11].

For a given distillation column, the reflux ratio is defined as flow returned per flow of top product removed [13]:

$$R_f = \frac{f_r}{f_p} \qquad 15$$

Where

R_f = Reflux ratio [-]

f_r = Flow returned as reflux [m^3/h]

f_p = Flow of top product removed [m^3/h]

The two extreme ends of reflux ratio are total reflux and minimum reflux. Total reflux describes the situation where all the condensate from the top is returned to the column., and no feed is added or product removed. On the other hand, minimum reflux occurs when no condensate is returned, and

the number of stages required in the column is infinite. This is because more reflux requires less stages to achieve separation, while less and less reflux requires more and more stages, until minimum reflux needs infinite stages [13].

Distillate describes the top product leaving the column, as shown in Figure 2, and it may be liquid, vapor or both [14]. The distillate to feed ratio is defined as the ratio of distillate flow to feed flow:

$$D = \frac{f_d}{f_f} \tag{16}$$

D = Distillate to feed ratio [-]

f_d = Distillate flow [m^3/h]

f_f = Feed flow [m^3/h]

2.3 Cooling tower

A cooling tower is a device that takes advantage of water evaporation and heat exchange between water and air to cool down hot water. It is widely used in industry to keep industrial equipment at acceptable operating temperatures. Figure 3 shows the components of an industrial cooling tower, specifically one using mechanical draft [15].

Inside a cooling tower, hot water encounters relatively dry, ambient air. In this exchange, small amounts of water will evaporate and cool down the water, a process that is enhanced by the induced draft of the tower. The hot water entering the tower is sprayed in with nozzles over a certain area of fill material that slows down the water. Water and air meet inside the fill material, where the cooling takes place. The fill material is designed to allow maximum exposure between air and water, with a large surface area and a maze of pathways [16].

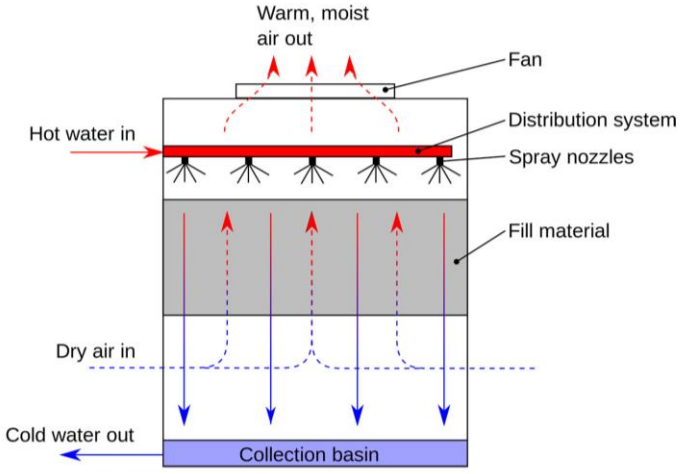

Figure 3: Fundamental components of a cooling tower [16].

There are many ways to distinguish different types of cooling towers, such as construction and air flow, but the most generalized is by draft. The three main draft types are atmospheric draft, mechanical draft and hybrid draft. Mechanical draft towers are the only relevant type for this thesis, and will be explained further [15].

Mechanical draft towers use fans to induce airflow through the tower, which lends them greater dependability than towers relying on atmospheric conditions. They also provide users with more control over the cooling power, by regulating the airflow. Where the fans are located in the circuit of a mechanical draft tower determines whether it uses forced draft or induced draft. Forced draft tower have fans located where the ambient air enters the tower, and often employ centrifugal blower fans. This saves space and allows for operation in high static pressure. These fans are, however, costlier than propeller fans. In addition, they are more prone to icing when they are located before the intake. Induced draft towers have fans on the exiting air stream, providing more protection against icing. Having fans at the discharge stream also reduces low-pressure areas at the inlets [15].

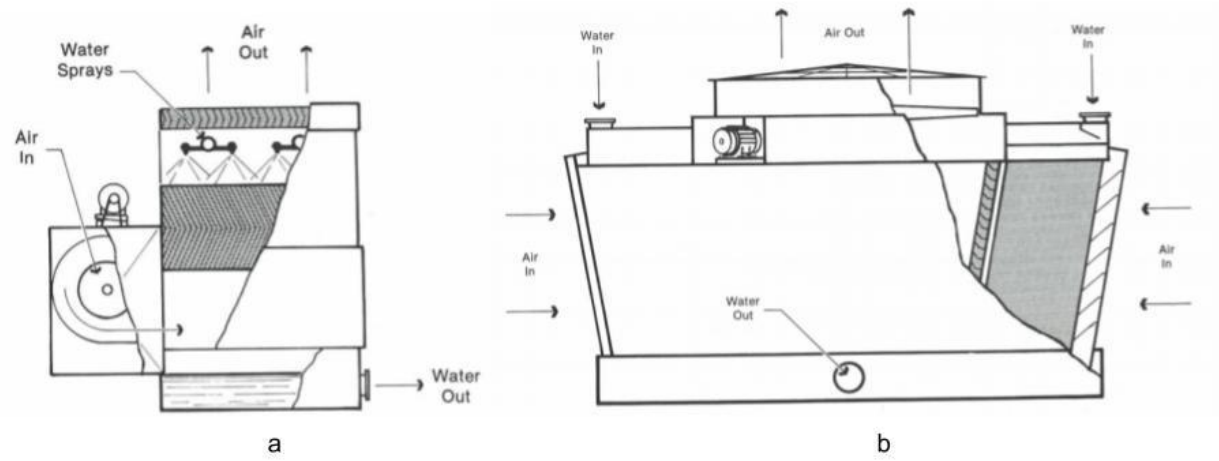

Figure 4: forced draft (a) and induced draft (b) cooling towers [15].

The final cooling tower characterization covered here is by air flow and includes crossflow and counterflow. In a crossflow cooling tower, the fill material is located in such a way that air flows horizontally through it. Water falls vertically down through the fill material, causing the air and water to cross flows. The hot water is fed onto the sections of fill material, alleviating the need for a pressure spray system. Counterflow towers, on the other hand, has air move up through the fill material vertically, while water falls downward vertically, as seen in Figure 5 [16].

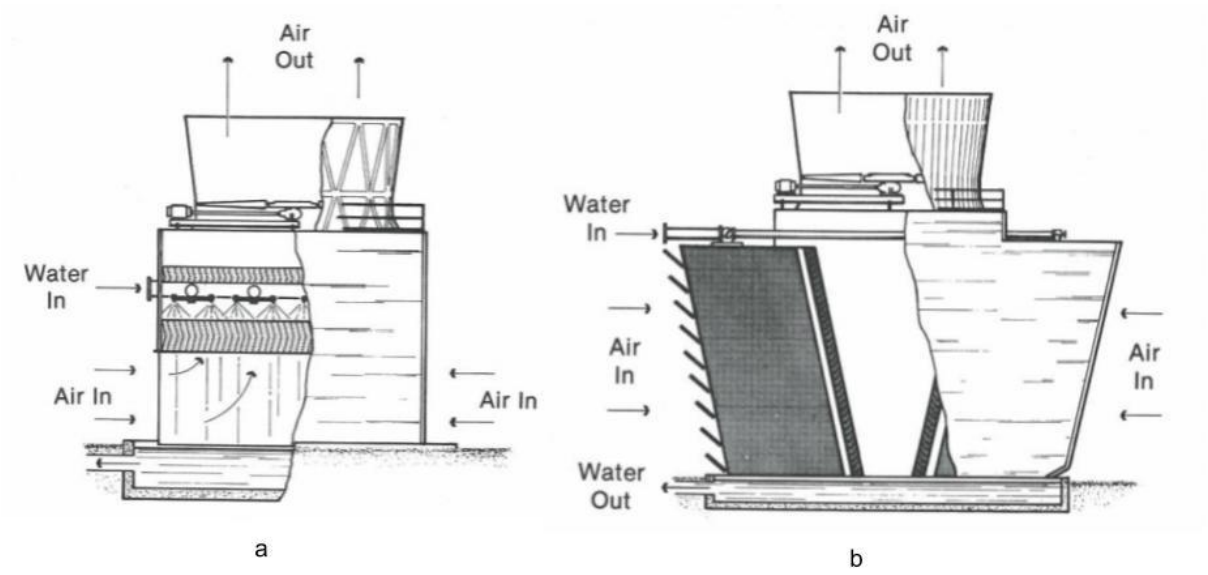

Figure 5: counterflow (a) and crossflow (b) cooling towers [15].

2.4 Equilibrium stages

Duffy [13] presents a method to find the number of equilibrium stages in a column using the McCabe-Thiele design method. This first requires the VLE diagram of the mixture in question. According to Price [17], the VLE diagram can be acquired by either experiment, calculation or in published sources. The water-air mixture of a cooling tower is not a typical case study regarding separation. Because of this no previous experiments or sources describe it, and the VLE diagram must be found by calculation. Obtaining the VLE diagram for a given mixture by calculation is a process requiring several steps and background knowledge, which will be presented here [18].

If the VLE diagram is not available for the given mixture, a Txy (Temperature x, y) diagram or a Pxy (Pressure x, y) diagram can be used to acquire it. The diagrams, as shown in Figure 6, represent pressure or temperature on the vertical axis, and mole fractions on the horizontal axis. The mole fractions range from 100 % of x and 0 % of y at the axis origin to 0 % of x and 100 % of y at x = 1.0. The method for finding the VLE in this thesis uses the temperature diagram. With it, the VLE diagram can be found by reading of the corresponding mole fractions of different temperatures.

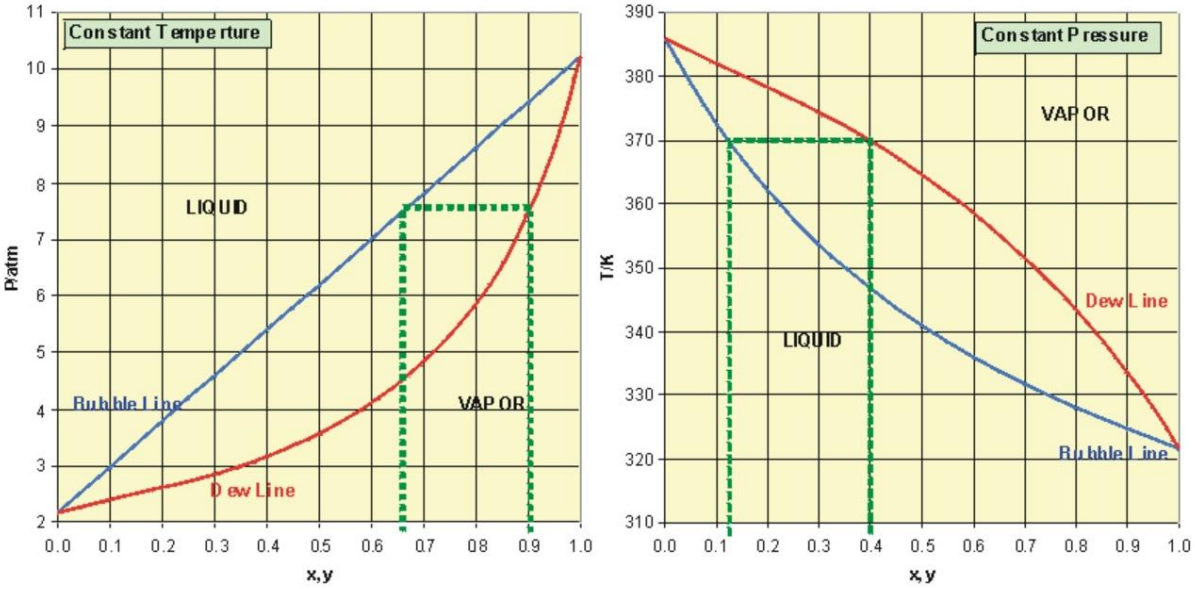

Figure 6: Pxy and Txy diagram[19]

To plot the Txy diagram, the boiling points of each component are used to create the end points. The boiling point of component *x* is where the starting point of both the bubble line and dew line. In Figure 6, the diagrams show a mix of pentane and heptane, with pentane as the lowest boiling point and heptane as the highest.

The bubble and dew line on the Txy diagram can be found by following *Raoult´s law* on vapor pressure. It only works on ideal mixtures, which don´t exist, but the law becomes more accurate the closer to ideal a mixture is. The law states that [18]:

$$p_A = x_A P_A^0 \quad (17)$$

And

$$p_B = x_B P_B^0 \quad (18)$$

Where

p_A = Partial vapor pressure of component A [atm]

x_A = Liquid mole fraction of component A [-]

P_A^0 = Vapor pressure of pure component A [atm]

p_B = Partial vapor pressure of component B [atm]

x_B = Liquid mole fraction of component B [-]

P_B^0 = Vapor pressure of pure component B [atm]

The total vapor pressure can be found by the following equation:

$$p_{tot} = p_A + p_B \quad (19)$$

Where

p_{tot} = Total vapor pressure [atm]

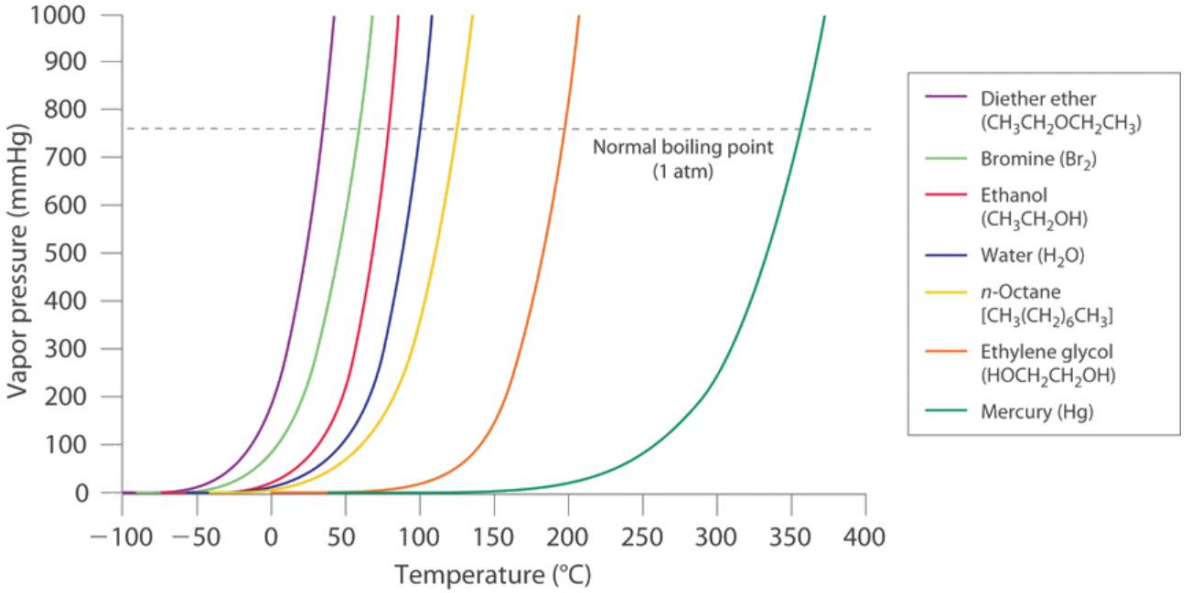

Figure 7: Relationship between vapor pressure and boiling point of different substances [20]

When the vapor pressure of a substance reaches the surrounding pressure, it will start to boil. Different substances have different boiling points, which will affect the resulting boiling point of a mixture. The vapor pressure of a substance depends on the fraction of molecules that have enough kinetic energy to escape the liquid state. This fraction is heavily dependent upon temperature, which can be seen increasing exponentially in Figure 7 [20]:

The Txy diagram of a given mixture can be found by calculating the vapor pressure of both substances in the mixture over a range of temperatures. The Antoine Equation can be applied to find vapor pressure and is given by [21]:

$$\log P_v = A_n - \frac{B_n}{C_n + T} \qquad 20$$

Where

P_v = Vapor pressure [mmHg]

A_n = Constant

B_n = Constant

C_n = Constant

A_n, B and C are the Antoine constants for a certain substance over a given temperature range. The units for pressure and temperature depend on what the constants are specifically tabulated for.

By reformulating eq. (20) to a temperature-explicit form, it can be expressed as:

$$T = \frac{B_n}{A_n - logP} - C_n \qquad 21$$

2.4.1 VLE diagram

Figure 8 shows a typical VLE diagram. It describes a mixture at constant pressure, where each point along the curve is a different temperature. As a rule of thumb, the larger the area between the x-y line and the curve, the more effective distillation will be at separating the components [17].

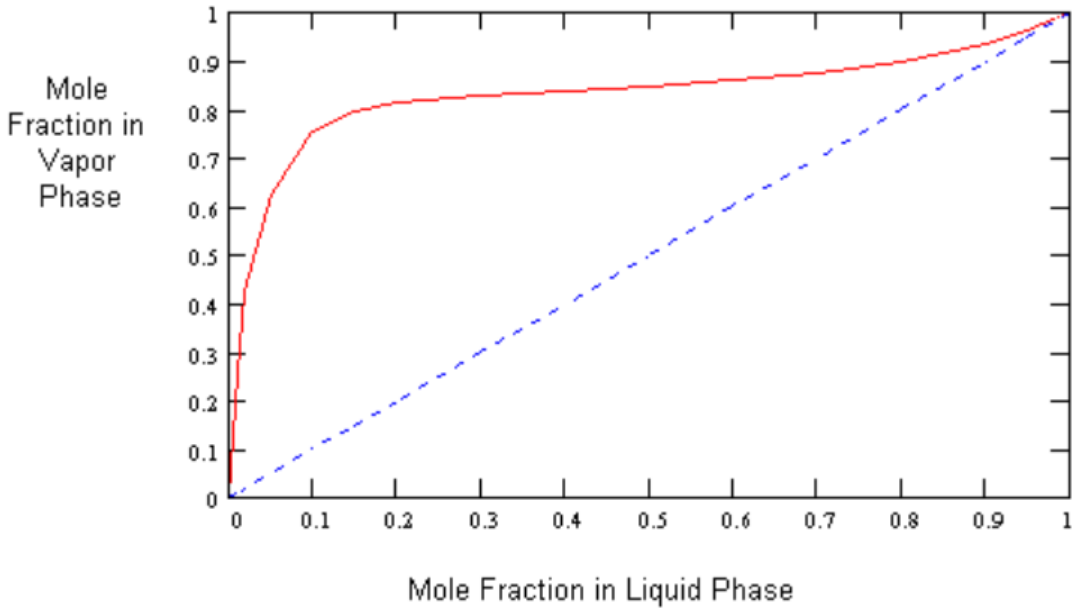

Figure 8: Example VLE diagram [17]

2.4.2 The McCabe Thiele method

McCabe and Thiele published a graphical method to find minimum reflux and number of equilibrium stages for a distillation column in 1925. Seader and Earnest [22] argues that computer methods are easier to use, but that the McCabe-Thiele method clearly demonstrates the main parts of distillation in a visual manner [22].

The McCabe-Thiele method makes the following assumptions about the system [13]:

- Constant molal overflow
- Column has no heat loss

Constant molal overflow means that the liquid and vapor flows in the rectifying section (above feed stage) and in the stripping section (under feed stage) are constant [23]. In other words, the number of molecules that evaporate and condense in each section is the same [24].

There is also a set of specifications that are necessary to know before using this method:

- Total feed rate
- Mole-fraction of the composition in the feed stream
- Operating pressure
- Mole-fraction in the distillate and bottoms
- Reflux to minimum reflux ratio

The first step of the McCabe-Thiele method is to have the VLE data of the mixture on an x-y diagram. To demonstrate the method, a benzene-toluene mixture showed in Figure 9 will be used.

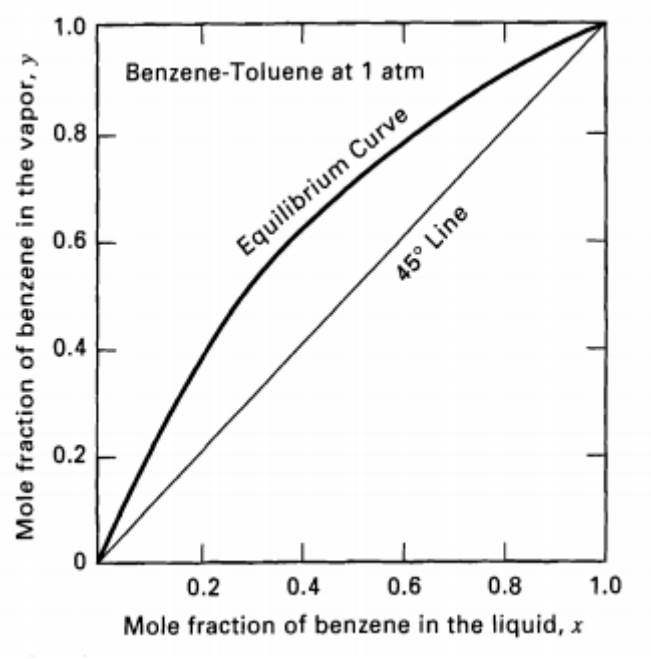

Figure 9: VLE diagram of benzene-toluene [22]

When the VLE diagram is available, the next step would be to pick the distillate composition and reflux ratio to find rectifying line. Distillate composition, X_D, is the amount of benzene in the distillate. Reflux ratio is given by eq. (15). The rectifying line is described as [13]:

$$Slope = \frac{R}{R+1} \tag{22}$$

Alternatively, the rectifying line intersection with the vertical line can be found by [13]:

$$\frac{X_D}{R+1} \tag{23}$$

Where

X_D = Distillate composition [-]

A typical value for reflux when using this method is 1.1 to 1.5 times minimum reflux. For the purposes of this example, a reflux ratio of 1.5 and a distillate composition of 0.8 are used. In a graphical context, minimum reflux is when the stripping line and rectifying line intersect on the equilibrium curve [13].

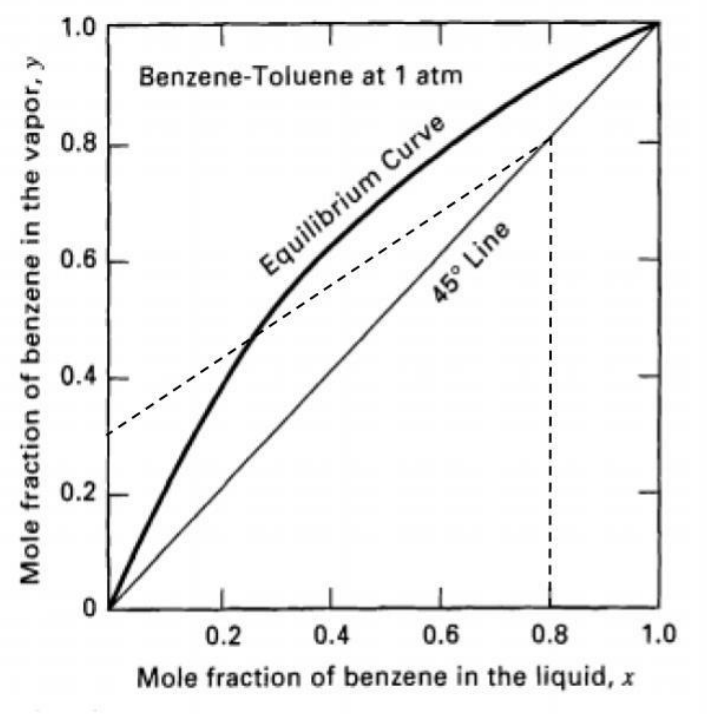

Figure 10: VLE with rectifying line [22]

The intersection across the vertical line according to eq. (23) is 0.32, which is shown in Figure 10. The rectifying line is the stipulated line that runs from the x-y line to the vertical line.

The next step would be to find the stripping line. In order to find it, the bottoms composition, X_B, and the boilup ratio, V_B, are necessary specifications. The boilup ratio describes how much liquid that is boiled back into the column as vapor to how much is removed in bottoms as liquid [13]:

$$V_B = \frac{f_u}{f_o} \tag{24}$$

Where

V_B = Boilup ratio [-]

f_u = Boilup [m^3/h]

f_o = Bottoms [m^3/h]

The slope of the stripping line is defined as: [13]

$$Slope = \frac{V_B + 1}{V_B} \tag{25}$$

Because distillate composition is 0.8, the bottoms composition is 0.2. With the knowledge that the stripping line starts from where the bottoms composition meets the x-y line, where the stripping line crosses the vertical line can be found [13]:

$$y_D = \frac{V_B + 1}{V_B} x_b + b \tag{26}$$

Where

y_D = Stripping line [-]

x_b = Mole fraction of benzene [-]

b = Constant [-]

For this example, boilup ratio is set to 1. With the information that when x=0.2, y=0.2, the intersection can be found:

$$0.2 = \frac{1+1}{1} * 0.2 + b \rightarrow b = -0.2 \quad (27)$$

The stripping line can now be added to the VLE diagram, as shown in Figure 11.

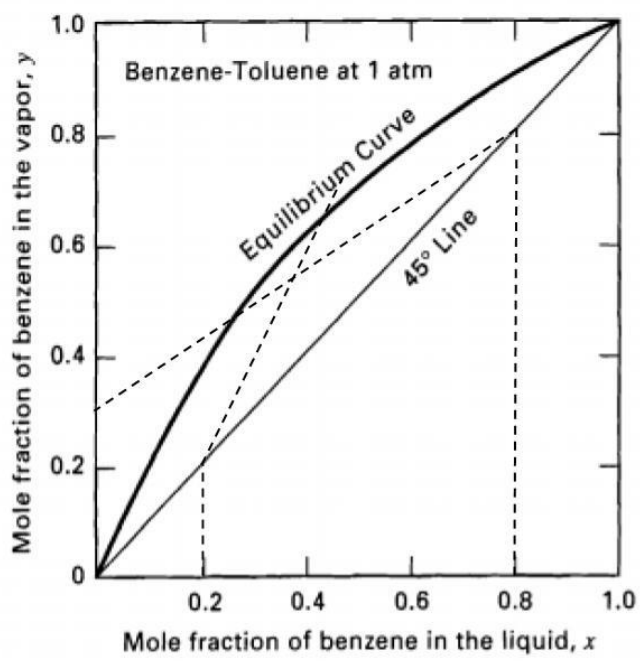

Figure 11:VLE with rectifying and stripping line [22]

With both rectifying and stripping line available, the process of finding the number of stages can be initiated. Start from where the distillate composition meets the x-y line and step off until the intersection of stripping and rectifying line is passed. Then step off using the stripping line [13].

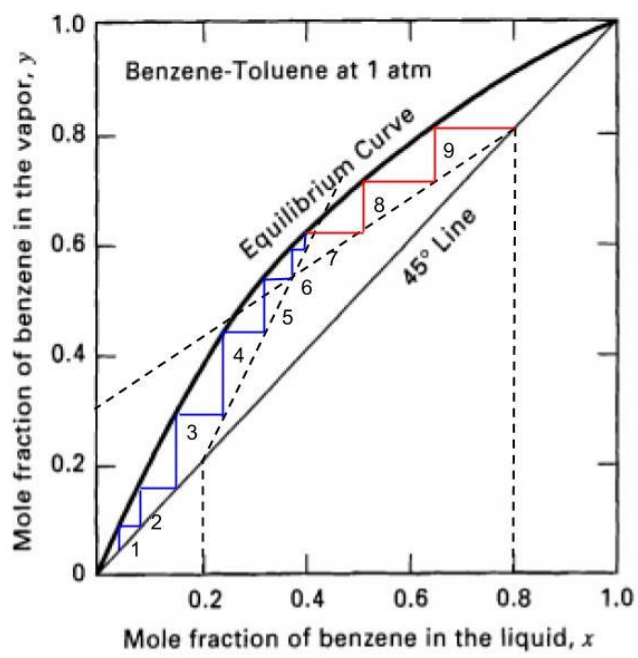

Figure 12: VLE with number of stages [22]

Figure 12 shows the number of stages calculated from the stepping process, with the red steps following the rectifying line and the blue following the stripping line. This gives the total number of equilibrium stages: 9. If the goal is to find the number of actual plates in the distillation column, the plate efficiency can be used in the following equation [13]:

$$N_p = \frac{N_e}{\eta_p} \qquad 28$$

Where

N_p = Number of plates [-]

N_e = Equilibrium stages [-]

η_p = Plate efficiency [-]

The reboiler will act as one ideal stage, it has to be subtracted to get the correct number of theoretical plates [13].

3. Methods

3.2 Heat loss calculations

The heat loss from the aluminum holding tanks and chutes at Chassix will be presented in this chapter. Finding the heat loss will be approached in two different ways, the first being calculation made just with the inner temperature, making necessary assumptions. The second will be calculations after measuring the surface temperature of the chutes and a holding tank.

3.2.1 Initial calculations

Some initial geometrical calculations of the tanks and chutes are necessary before starting on the heat loss calculations. Volume, wall area and wall length are presented in Table 1. Volume is based on amount of aluminum in tanks and chutes and aluminum density. The walls of the holding tanks and chutes consist of firebrick and fiber insulation.

Table 1: Geometrical values

	Volume [m^3]	**Wall area [m^2]**	**Wall length [m]**
Tank (per tank)	4.615	2.772	1.665
Chute (per meter)	0.0346	0.1062	0.3259

Insulation in chutes are 12-15 *cm* in total, while tanks have approximately 40 *cm* [25]. A basis of 8 cm firebrick and 5 *cm* fiber insulation is assumed in the chutes. For tanks, 15 *cm* of fiber and 25 *cm* of firebrick is assumed. 1 *m* of chute contains approximately 90 *kg* of Aluminum, while one tank contains roughly 12 000 *kg* [25].

Table 2: Insulation layer values for chutes and tanks

	Heat transfer coefficient [W/m*K]	**Length [m]**	
	Chutes	Tanks	Chutes
Firebrick	0.3	0.25	0.08
Fiber insulation	0.04	0.15	0.05

The length of each insulation layer in Table 2 is assumed, as well as a squared geometry for simplicity. Average heat transfer coefficient is necessary for the heat loss calculations and was found to be 0.2025 *W/m*K* for the tanks and 0.173 *W/m*K* for the chutes.

3.2.2 Calculations from assumptions

Chassix receives their aluminum in liquid form at 730 *°C* and employs heating elements in the holding tanks, chutes and injection machines, which contain aluminum all year. For the purposes of these calculations, an ambient temperature of 20 *°C* is assumed.

In addition to the holding tanks and chutes examined in this chapter, Chassix has a 1000 *kg* tank acting as a temporary holding tank and a crucible with 2000 *kg* capacity under each molding machine. The amount of liquid aluminum in these is controlled by the production rate. Their energy consumption has not been calculated in this thesis.

The easiest way to calculate heat loss through a multi-layered wall is to imagine the wall as an electric network, with several resistances in series. Thermal resistance in the wall layers can be calculated as heat transfer by conducting, using eq. (13):

$$R = \frac{x}{kA}$$

Convection and radiation on the outside wall, which is in contact with air, can be accurately calculated by determining the heat transfer coefficient*, h*. However, the combined heat transfer coefficient of convection and radiation can also be assumed in a reasonable range, making the calculations much simpler. Thermal resistance of convection and radiation can then be found according to eq. (3):

$$R_{conv} = \frac{1}{hA_b}$$

To calculate the heat transfer without knowing the outer surface temperature, the combined heat transfer coefficient of convection and radiation must be assumed. Considering the heat transfer coefficient for convection and radiation combined outside a window with a 30 *°C* drop is 40 *W/m*K* [7], the number in this scenario is probably higher. However, looking at equation for convection resistance, eq. (3) and heat transfer through a multi layered wall, eq. (14), the coefficient has minimal impact on the overall heat transfer. By using a heat transfer coefficient of 70 *W/m*K*, the resistance from convection and radiation can be estimated.

Once all thermal resistances have been determined, the heat transfer from the liquid aluminum to ambient air can be determined by using eq. (14):

$$Q = \frac{T_i - T_j}{R_{total}}$$

Total heat loss from holding tanks is now given by:

$$E_{loss} = Q * h \qquad 29$$

3.2.3 Calculations from measurements

To calculate the heat loss from the chutes and tanks more accurately, the surface temperature of both were measured. The measurements were carried out 18.04.2018 at Chassix. An infrared (IR) thermometer was used to measure the surface temperatures, which are shown in Table 3. Four temperature measurements were taken of the chute and two of the tank. The averages of these measurements are also shown.

Table 3: Temperature measurements in degrees Celsius

	Measurement 1	Measurement 2	Measurement 3	Measurement 4	Average
Chute	48.4	44.6	45.7	47.7	46.6
Tank	55.0	54.0			54.5

As covered in the theory chapter, heat loss always occurs in three different ways, all of which have to be included to create a result that is as accurate as possible. In the previous chapter, these losses were added together under the concept of thermal resistance. Here, however, they can be calculated separately because the surface temperature has been measured.

Figure 13: View of a chute carrying liquid aluminum

The first heat loss area is conduction, which is given by Eq. (1):

$$Q_{cond} = kA\left(\frac{T_t - T_s}{L}\right)$$

Convection

The values in Table 4 are necessary for the convection heat loss calculations made throughout this chapter.

Table 4: Values for convection [8]

	Value
g	9.81 m/s^2
v	14.77*10^{-6} m^2/s

Pr	0.69
k	0.0261 W/m*K

To find the heat transfer coefficient, the Rayleigh number is the first necessary value. By replacing the Grashof number in eq. (5) with its definition in eq. (8), the following equation can be used:

$$Ra_x = Gr_x Pr = \frac{\beta \Delta T g L^3}{\nu^2} Pr \quad (30)$$

The resulting Rayleigh number found in these calculations for the tanks is $1.593*10^{10}$. This number is larger than the limit of $Ra_x \leq 10^9$. Mills [9] provides another Nusselt number equation than eq. (10) for $10^9 \leq Ra_x \leq 10^{12}$, but these equations are not clearly separated when the Rayleigh number is close to 10^9. This gives eq. (10) validity even if the result overshoots the boundary slightly.

Reference temperature:

$$T_r = T_s - \alpha(T_s - T_e)$$

This can be used to find the volumetric coefficient of gas:

$$\beta = \frac{1}{T_r}$$

Prandtl number function value:

$$\Psi = \left[1 + \left(\frac{0.492}{Pr}\right)^{\frac{9}{16}}\right]^{-\frac{16}{9}}$$

The Nusselt number can then be found from eq. (10):

$$Nu_L = 0.68 + 0.670(Ra_x \Psi)^{\frac{1}{4}}$$

With, this value eq. (11) can be used to find heat transfer coefficient:

$$h = \frac{k}{L} Nu_L$$

Convective heat loss from the chutes and tanks can be calculated from eq. (2), assuming the same ambient temperature across all surfaces.

$$Q_{conv} = hA(T_s - T_{surr})$$

Finally, radiation losses can be found from eq. (12):

$$Q_e = \varepsilon \sigma A_s (T_s^4 - T_{surr}^4)$$

The emissivity of the tanks, which are made of steel, is assumed to be 0.80 (between polished and weathered stainless steel) [10].

3.3 Cooling tower simulation

3.3.1 Aspen Plus

Aspen Plus is widely used in industry, particularly in chemical engineering [26]. It is a powerful tool to use when analyzing complex processes, but it requires a considerable amount of prior knowledge about thermodynamics, industrial devices and chemistry. Necessary background knowledge depends, of course, heavily upon what process you wish to create a model of and simulate in Aspen. The simulation presented in this thesis are of a cooling tower, which is not readily available in Aspen. Creating it is, therefore, a process of research and trial and error. General information about Aspen Plus will be presented in this chapter, as well as the process to create and run the models.

The user can create his own process model based on a wide selection of units in Aspen Plus. As Aspen does not provide the process design, it is necessary for the user to first create one, and then select the appropriate operating conditions and thermodynamical properties. Aspen Plus will then predict the performance of the model using mathematical models [26].

Several assumptions are necessary to make when setting up the model in Aspen Plus, including:

- No heat loss from the cooling tower to surroundings
- Pressure drop across the tower is zero
- Steady state operations

When building a model in Aspen Plus, choosing the correct property method will influence the accuracy of the results, making it an important decision. The most basic property method is IDEAL, which includes several underlying relationships:

- Ideal mixing in fluid
- Ideal activity coefficient for liquid phase
- No intermolecular interactions and molecules are without size
- Ideal gas EOS (Equation of State) for vapor phase

Ideal gas EOS for vapor state means the system is following the ideal gas law [27]:

$$PV = nRT \tag{31}$$

Where

P = Pressure [Pa]

V = Volume [m^3]

n = Amount of gas [mol]

R = Gas constant= 8.314 [J/K*mol]

Ideal models are suitable for mixtures with a low grade of polarity, such as paraffins, aromatics or ethers. A mixture can have a high degree of ideality if the polarities cancel each other out [26].

Eden [26] recommends the ideal gas law when the pressure in the system is low, which is the case with the cooling tower at Chassix. The induced draft affects the pressure difference across the tower slightly, but Queiroz et al [3] argued that pressure drop across the tower could be neglected when the

model is not being used in design. They modeled an existing induced draft, counter flow cooling tower in steady-state operation, which is similar to the cooling tower system considered in this thesis.

Queiroz et al [3] also proved that with cooling towers operating at such low temperature and pressure, simulating the model with the IDEAL property method yielded the same output values as when using NRTL (Non-Random Two-Liquid), a property method for non-ideal solutions. They based this on the assumption that the water stream was free from impurities, as it would not have a significant impact on the steady-state properties [3].

3.3.2 Simulation

When creating the model for the cooling tower system, the system properties had to be specified. SI (International System Units) was the chosen global unit. The other system property is the method property, which was set to IDEAL, based on the arguments of Queiroz et al [3] and Eden [26].

When creating a new model in Aspen Plus, the program will automatically prompt the user to the next step. After selecting property methods, the next prompted step is to input all the necessary components that the model will require. In this simulation, a water stream free of impurities is assumed for simplicity. Figure 14 shows the components used in this simulation, water and air.

Component ID	Type	Component name	Alias
AIR	*Conventional*	AIR	AIR
WATER	*Conventional*	WATER	H2O

Figure 14: Components

A cut-out of the model flowsheet is shown in Figure 15. When constructing a flowsheet to represent a cooling tower in Aspen Plus, a replacement is necessary because there is no built-in block for cooling towers. The RadFrac-block is usable as a representation if certain adjustments and assumptions are made. In Aspen Plus, the RadFrac-block represents a distillation column, which is necessary to understand before proceeding with building the model.

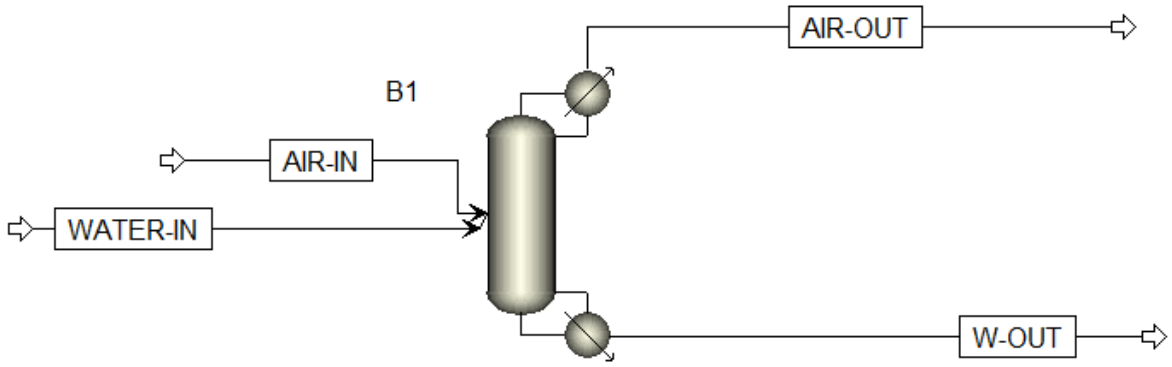

Figure 15: Cooling circuit flowsheet

The cooling tower at Chassix was decommissioned during the writing of this thesis, so arbitrary values of 50 *l/s* was used for the air flow. On the other hand, the water flow in the model was based on earlier, steady state values at Chassix, 17.7 *l/s*. Figure 16 shows the top and bottom stages of the RadFrac block

in Aspen Plus. Water enters at stage 1 and exits at stage 6, while air enters at stage 6 and exits at stage 1.

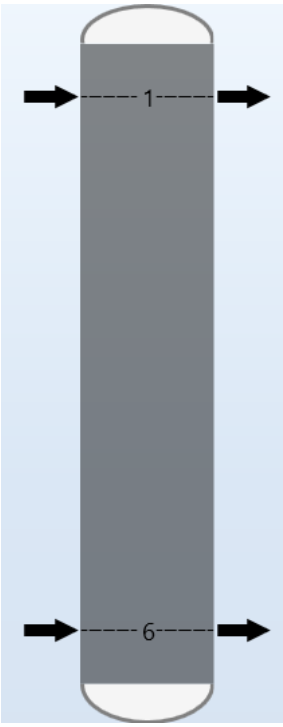

Figure 16: Column internals

3.3.3 Equilibrium stages

For water, Yaws [28] provides the following Antoine constants for water within a temperature range of 0.01 °C to 373.98 °C:

A_n = 8.05

B_n = 1723.64

C_n = 233.08

The Antoine constants for air, however, are very difficult to procure. Mainly because vapor pressure is a thermodynamic property most often used to describe liquids and their boiling points. Also, when using a VLE diagram in separation calculations, substances that are in liquid form at mild temperatures and pressures are traditionally used.

This thesis attempts to find the Antoine constants for air by using the correlating pressures of air at low temperatures. Using the temperature-pressure tabulated values [29] that apply along the boiling curve, the boiling curve of air is created in Figure 17.

One assumption that simplifies this process is to assume that the vapor pressure of a gas is equal to the normal pressure of the gas. By looking at Figure 7, It is clear that the vapor pressure increases beyond that of the boiling point, following the usual correlation of temperature and pressure of a gas. Following this assumption, the graph in Figure 17 can be used to estimate the theoretical Antoine constants of air.

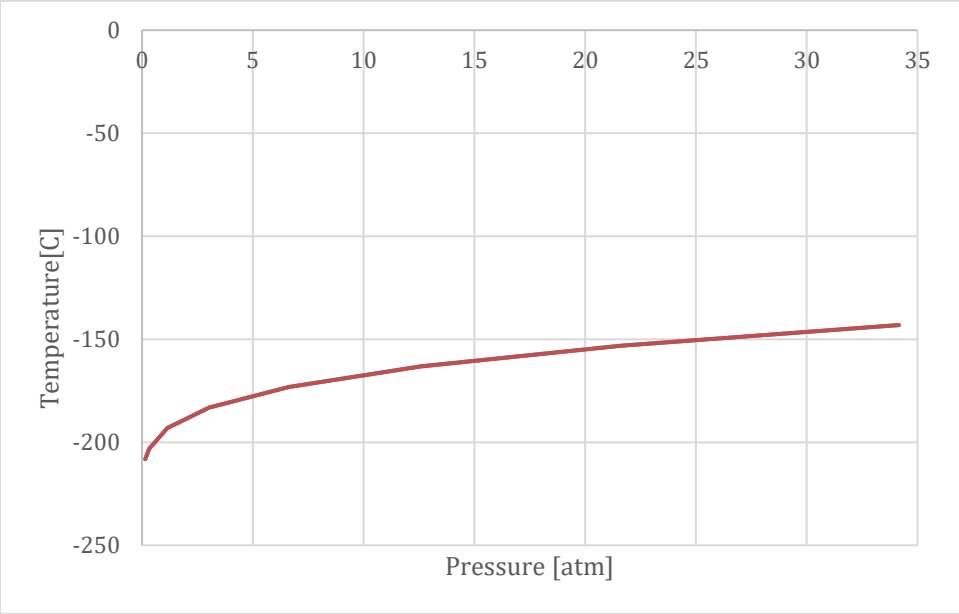

Figure 17: Pressure and temperature of air at boiling curve [29]

The problem was set up as a minimizing function in Excel. Eq. (21) was used to estimate the temperature based on the initial Antoine Constants:

$$T(estimated) = \frac{B_n}{A_n - logP} - C_n$$

The difference between T(estimated) and the actual temperature, squared, in the graph was then added:

$$T(diff) = \big(T(actual) - T(estimated)\big)^2 \tag{32}$$

One T(diff) was calculated for each data point of temperature and summarized as the total temperature difference, which was finally minimized using Excel Problem Solver. The resulting Antoine constants for air were:

A_n = 3.91

B_n = 310.73

C_n = 273.69

The sum of the temperature difference for these constants was 0.026, an acceptably low number.

With the Antoine constants for both air and water available, it now becomes possible to create the boiling line of a water-air mixture.

Assuming the total liquid mole fraction of water and air is 1 at all times, the mole fraction of water can be described as:

$$x_w = 1 - x_a \tag{33}$$

Where

x_w = Liquid mole fraction of water [-]

x_a = Liquid mole fraction of air [-]

Using eq. (17) and eq. (18), incorporated into eq. (19), the following equation is derived:

$$P_a^0 x_a + P_w^0 x_w = 1\ atm \tag{34}$$

Where

P_a^0 = Vapor pressure of pure air [atm]

P_w^0 = Vapor pressure of pure water [atm]

Substituting eq. (33) for water fraction in eq. (34) gives:

$$P_a^0 * x_a + P_w^0(1 - x_a) = 1\ atm \tag{35}$$

This equation can be manipulated into expressing the air fraction:

$$\frac{P_w^0 - 1}{P_w^0 - P_a^0} = x_a \tag{36}$$

The liquid mole fraction of air can now be used to plot the boiling line of the water-air mixture, along with temperature. For every temperature between the boiling points of air and water, the vapor pressure of air and water is calculated according to eq. (20).

In finding the dew line of the water-air mixture, it becomes necessary to expand on the previously used eq. (17) and eq. (18). As it was assumed that the total amount of liquid mole fraction always equaled 1, so can the vapor mole fraction in the vapor phase be assumed to equal 1:

$$v_a + v_w = 1 \tag{37}$$

Where

v_a = Vapor mole fraction of air [-]

v_w = Vapor mole fraction of water [-]

With this, *Raoult´s law* can be expanded to accommodate the vapor phase as well, assuming that the vapor phase corresponds to the pressure in the gas, while the liquid phase corresponds to vapor pressure. eq. (17) and eq. (18) can then be expressed as [30]:

$$v_a P = x_a p_a^0 \tag{38}$$

And

$$v_w P = x_w p_w^0 \tag{39}$$

It is now necessary to manipulate these equations to only include the vapor mole fractions. By dividing by vapor pressure, the liquid mole fractions are expressed as:

$$\frac{v_a P}{p_a^0} = x_a \tag{40}$$

And

$$\frac{v_w P}{p_w^0} = x_w \tag{41}$$

Following the assumption of eq. (37), that the sum of the liquid mole fractions is 1:

$$x_a + x_w = 1 \tag{42}$$

eq. (40) and eq. (41) can now be added together:

$$\frac{v_a P}{p_a^0} + \frac{v_w P}{p_w^0} = 1 \quad 43$$

Making this equation pressure-explicit yields:

$$P = \frac{1}{\frac{v_a}{p_a^0} + \frac{v_w}{p_w^0}} \quad 44$$

As with the boiling line, constant pressure of 1 *atm* is assumed. This turns eq. (44) into:

$$\frac{v_a}{p_a^0} + \frac{v_w}{p_w^0} = 1 \quad 45$$

To plot the mole fractions, it is necessary to create an equation that expresses either air or water mole fraction. Using eq. (37), water vapor mole fraction can be described as:

$$v_w = 1 - v_a \quad 46$$

This can be inserted into eq. (45):

$$\frac{v_a}{p_a^0} + \frac{(1 - v_a)}{p_w^0} = 1 \quad 47$$

To have this equation express vapor air mole fraction, all components must be multiplied by $p_a^0 p_w^0$:

$$\frac{v_a}{p_a^0} * p_a^0 p_w^0 + \frac{(1 - v_a)}{p_w^0} * p_a^0 p_w^0 = 1 * p_a^0 p_w^0 \quad 48$$

This gives:

$$v_a p_w^0 + (1 - v_a) * p_a^0 = p_a^0 p_w^0 \quad 49$$

By manipulating this equation, it eventually expresses vapor air mole fraction as:

$$v_a = \frac{p_a^0 p_w^0 - p_a^0}{p_w^0 - p_a^0} \quad 50$$

The Antoine constants for water used in calculating the boiling line are still valid here, as the temperature range is the same. The Antoine constants for air, however, were based on the temperature-pressure relationship along the boiling curve. To create more accurate constants for the dew line, the temperature-pressure relationship along the condensing line [29] for air is used. Figure 18 shows this information.

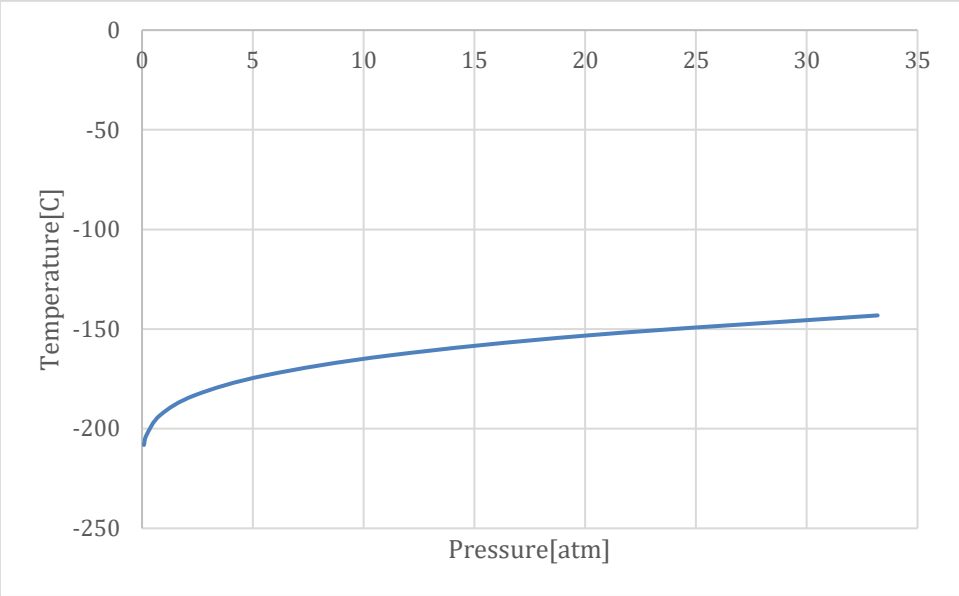

Figure 18: Pressure and temperature of air at condensing curve [29]

Similar to finding the Antoine constants for air at the boiling curve, Excel Problem Solver is used to minimize the difference between the tabulated temperature and the temperature given by eq. (21). The calculated Antoine constants are:

A_n = 4.06

B_n = 328.12

C_n = 272.21

As with creating the bubble line, eq. (20) was used to find vapor pressure of air and water across the temperature range. In addition, eq. (50) described the air vapor mole fraction, which was plotted with the temperature to create the dew line.

The VLE diagram of the air-water mixture can now be created according to the McCabe-Thiele method in the Theory chapter. Using the resulting diagram, however, will not follow the same approach because the graph does not follow a curved line. The VLE diagram will be presented in the Results and analysis chapter.

4. Results and analysis

4.2 Heat loss

4.2.1 Calculations from assumptions

Thermal resistance breakdown for holding tanks and chutes is shown in Table 5. These numbers are based on eq. (13).

Table 5: Thermal resistances

	Thermal resistance, wall [K/W]	Thermal resistance, convection and radiation [K/W]
Tanks	0.0396	$2.863*10^{-4}$
Chutes	0.0136	$2.242*10^{-4}$

Using the thermal resistance values, total heat loss for all three tanks and all 150 meters of chute is calculated from eq. (14). The result is shown in Figure 19. The combined heat loss is 69.14 *kW*.

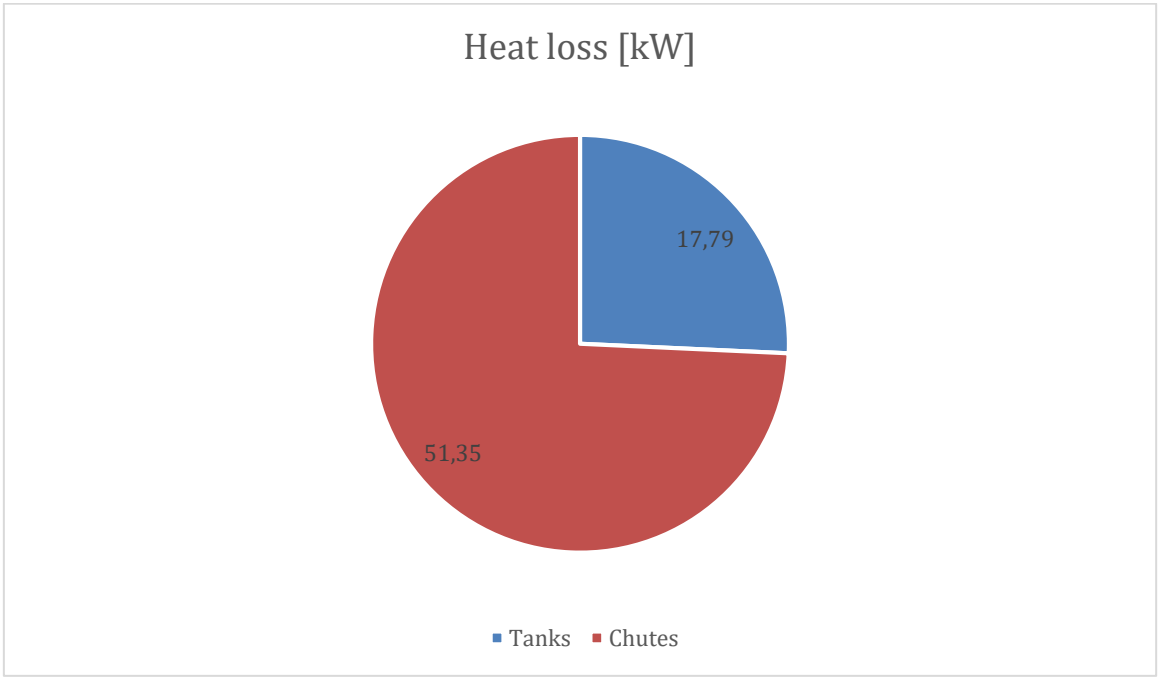

Figure 19: Heat loss from assumptions

4.2.2 Calculations from measurements

The values of the resulting heat transfer coefficients used in the heat loss calculations is shown in Table 6.

Table 6: Heat transfer coefficients

	Tanks	Chutes
Heat transfer coefficient [W/m²*K]	2.87	4.03

Heat loss from the tanks based on the measured surface temperatures is shown in Figure 20, broken into conduction, convection and radiation. Conduction is undoubtedly the most significant source of heat loss with 63 %, while convection and radiation each account for about the same amount of heat loss.

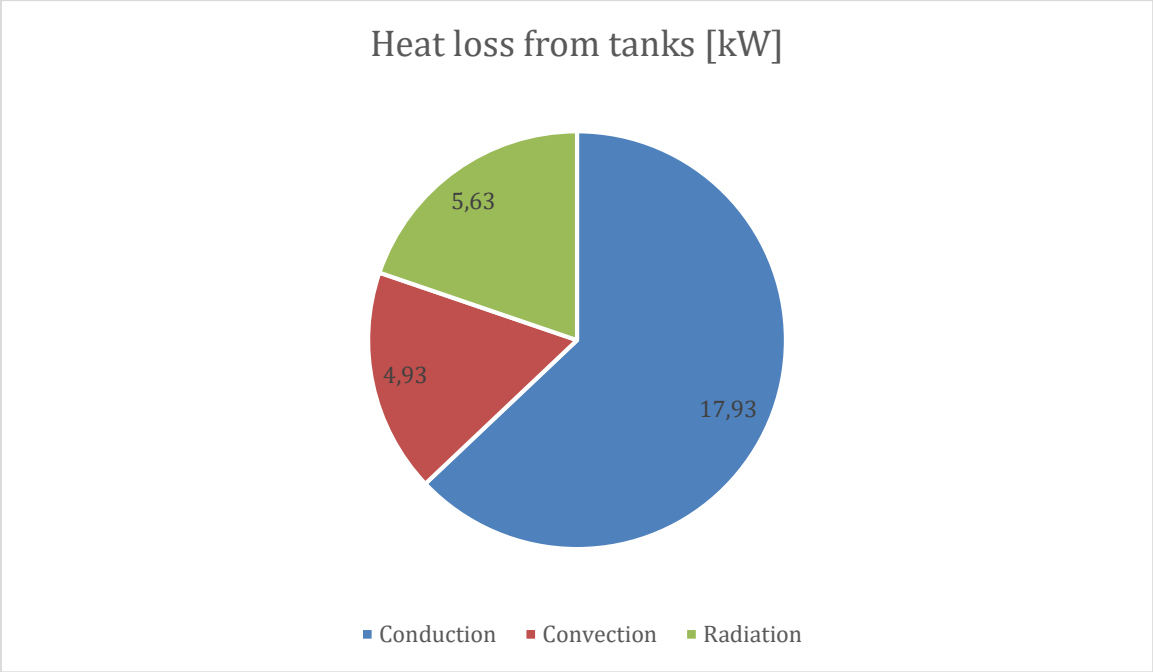

Figure 20: Heat loss from tanks based on measurements

Figure 21 shows how each type of heat loss relates to the surface temperature of the tanks. The conduction heat loss decreases as the surface temperature increases because the temperature difference between the inside and outside of the tank decreases.

The convection increases, but not linearly, because the Rayleigh number is dependent on both the temperature difference between surface and ambient temperature, as well the inverse of reference temperature. The inverse of reference temperature will cause the total convection heat loss to decrease with increases surface temperature, but not as much as the surface and ambient temperature increases.

Radiation is the type of heat loss that increases the most with increased surface temperature. As with conduction, there is only one variable, the surface temperature. The difference to conduction, however, is that the temperature difference increases. As the surface temperature is the only variable, and increases to the power of four, it can be seen from the Figure 21 that radiation increases more rapidly than convection. The emissivity constant varies widely for different materials, even for different types of steel, which the tank and chute surfaces are made of. The emissivity constant for the

calculation in this thesis was assumed to be between polished stainless steel and weathered stainless steel [10]. With different surface materials, the heat loss form radiation can change drastically. New galvanized steel, for instance, has an emissivity constant of 0.23, which would make radiation only cause 36.2 % of the heat loss with the current emissivity value of 0.8.

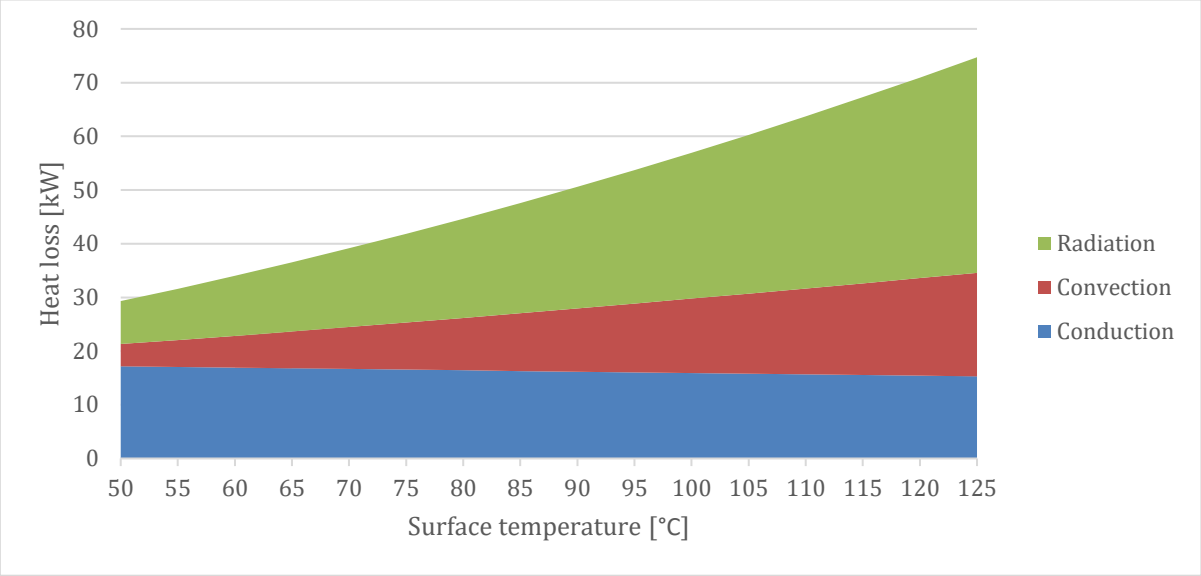

Figure 21: Heat loss from tanks based on surface temperature

The heat loss breakdown for the chutes can be seen in Figure 22. As with the tanks, conduction is the largest source of heat loss with 76 % of the total. The conductive heat loss from chutes is 2.8 times as high as for the tanks, which is significantly more than for convection and radiation, 1.4 and 1.57 respectively. This considerable difference comes mainly from the thinner walls of the chutes, 13 *cm* compared to the 40 *cm* of the tanks.

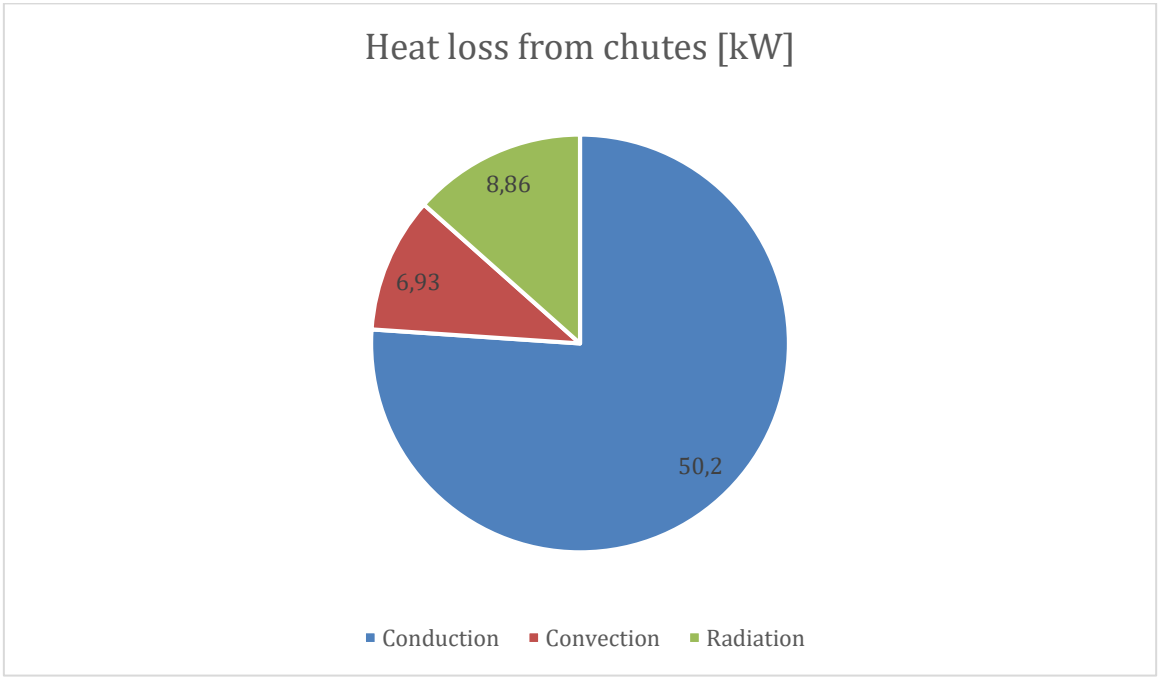

Figure 22: Heat loss from chutes based on measurements

How the different types of heat loss changes with increased surface temperature is shown in Figure 23. They follow the same trends as heat loss for the tanks.

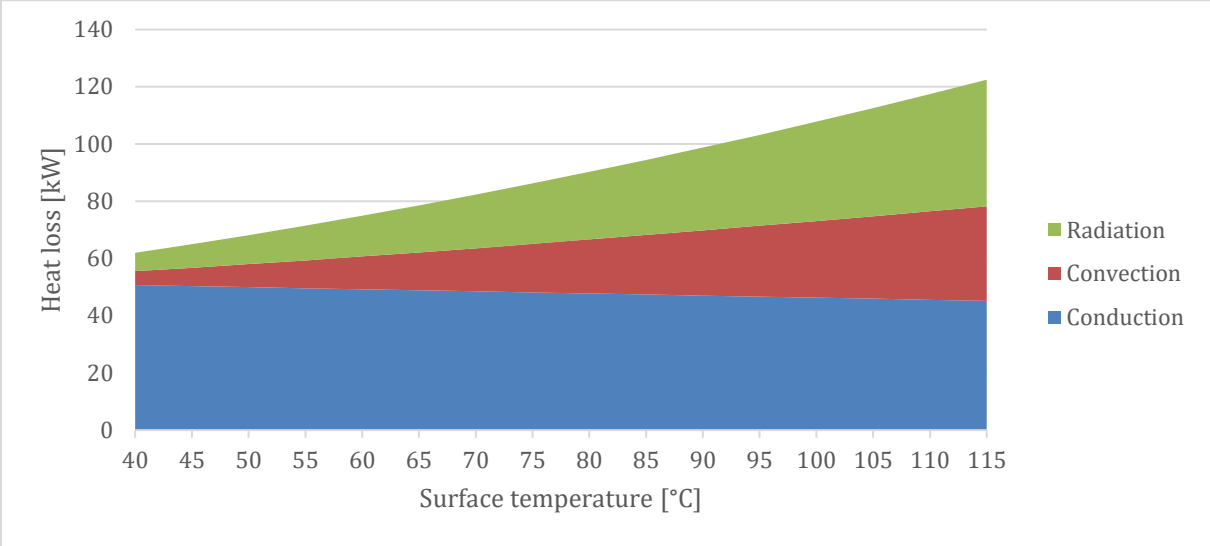

Figure 23: Heat loss from chutes based on surface temperature

How the heat loss is distributed between the tanks and chutes is shown in Figure 24. The total is 94.48 *kW*, of which tanks make up 30 % of the heat loss, while the chutes account for 70 %. This is close to the same distribution in the calculations based on assumptions, where there is a 26 % to 74 % split between tanks and chutes.

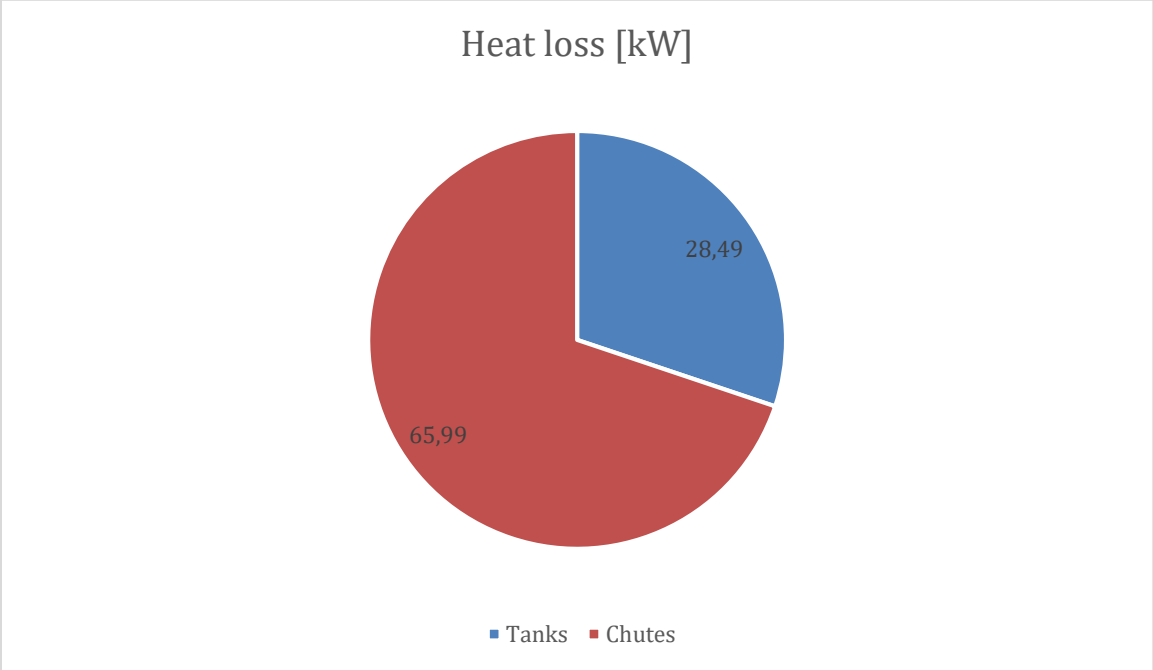

Figure 24: Heat loss from tanks and chutes

Total heat loss over a year is shown in Figure 25, with the heat loss from measurements broken down into its components. The combined heat loss based on measurements is 827.64 *MWh*, which is 36.65 % more than heat loss calculated with only thermal resistance at 605.65 *MWh*. It is difficult to say

which type of heat loss differs the most between the two methods, because thermal resistance without surface temperature only finds the total heat loss.

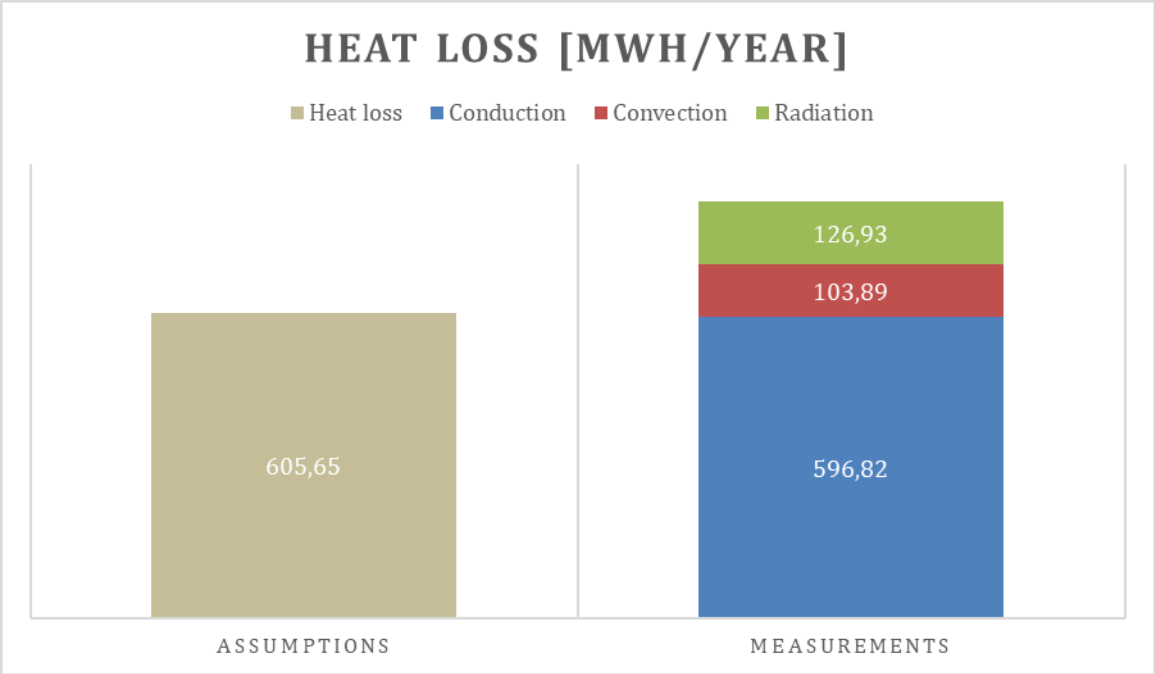

Figure 25: Heat loss from assumptions and measurements

With the energy lost through heat loss calculated in this thesis, as well as information gathered in the research project, mapped energy flow throughout different areas at Chassix is illustrated in Figure 26. The amount of electricity that makes up the entire flow is not the whole electricity consumption of Chassix, which was 24119 in 2016 [5].

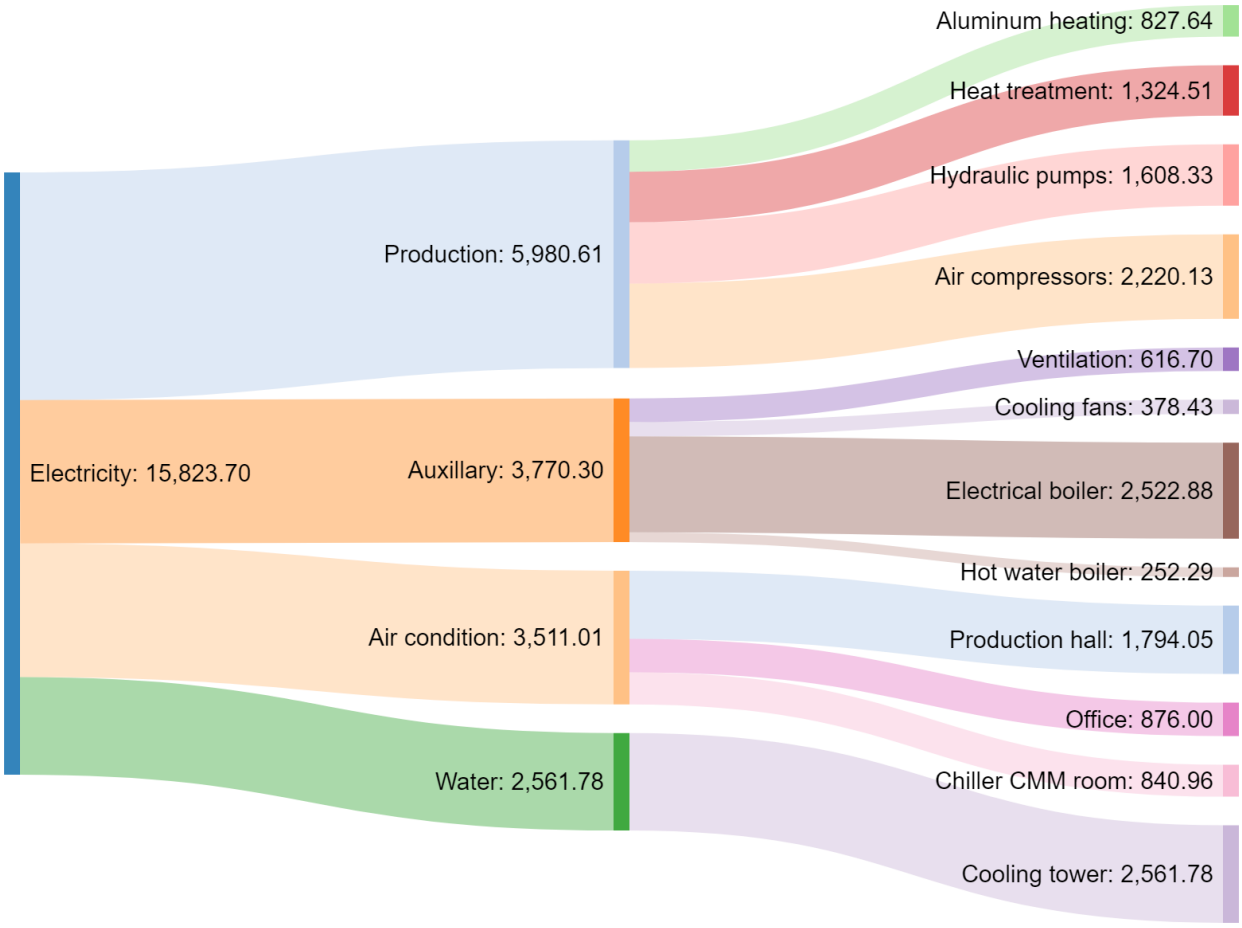

Figure 26: Sankey diagram of energy flow in MWh

4.3 Cooling tower simulation

4.3.1 Equilibrium stages

Figure 27 shows how the boiling line represents the mole fractions of water and air that is necessary to continually keep the vapor pressure at the surrounding pressure of 1 *atm*.

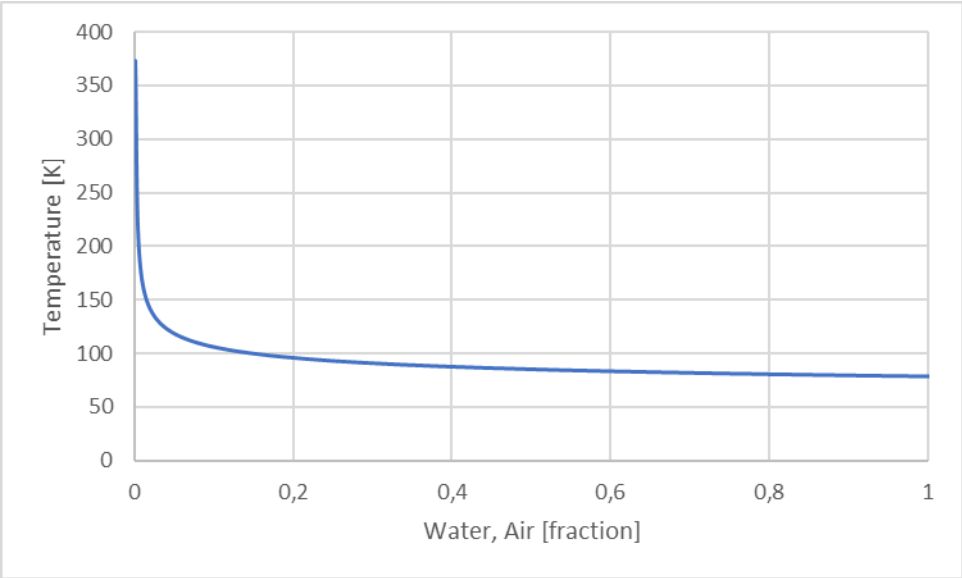

Figure 27: Boiling line of water-air mixture

The calculations and reasoning to find the dew line and bubble line for an air-water mixture yielded the graph in Figure 28. The two components have widely different boiling points, which is represented in the graph.

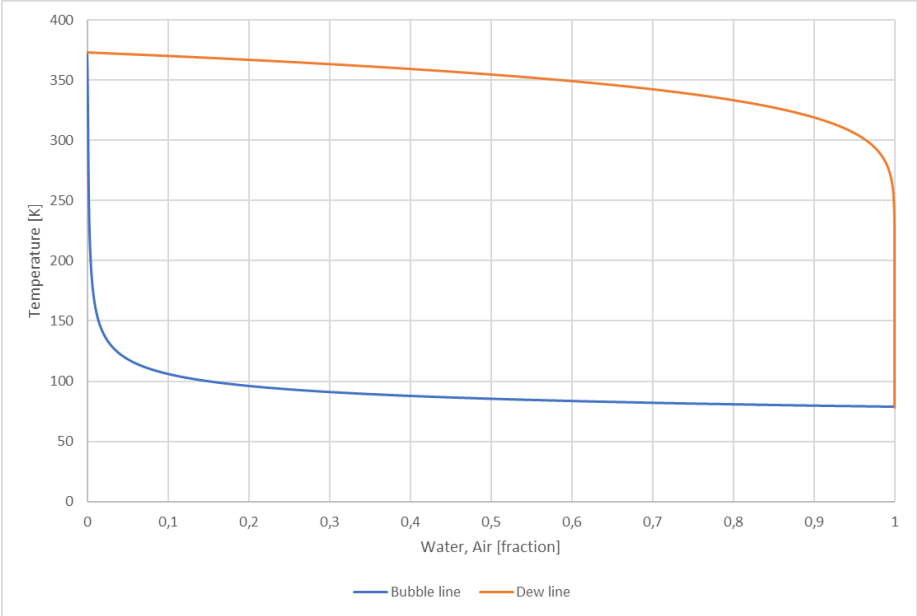

Figure 28: Txy diagram for air-water mixture

Once the Txy diagram for the water-air mixture is available, it is a simple process to create the VLE diagram. Figure 29 shows the VLE diagram made from the Txy diagram in Figure 28. The blue line shows the mole fractions of water and air in both liquid and vapor phase. For a VLE diagram, the further the

blue line is from the x-y line, the greater separation is achieved. For air and water, this shows clearly how difficult the two are to mix.

The VLE diagram is necessary to use the McCabe-Thiele method of finding equilibrium stages. However, when the graph is created, the vapor-liquid line closely hugs the vertical line. As the McCabe-Thiele steps off the line to count the number of stages, a line that moves closer and closer to the angular line in Figure 29, will have less and less stages. In theory, this means that the number stages become 1. This value is not usable in the simulation, which is why a number based on the results from Queiroz et al [3] was used.

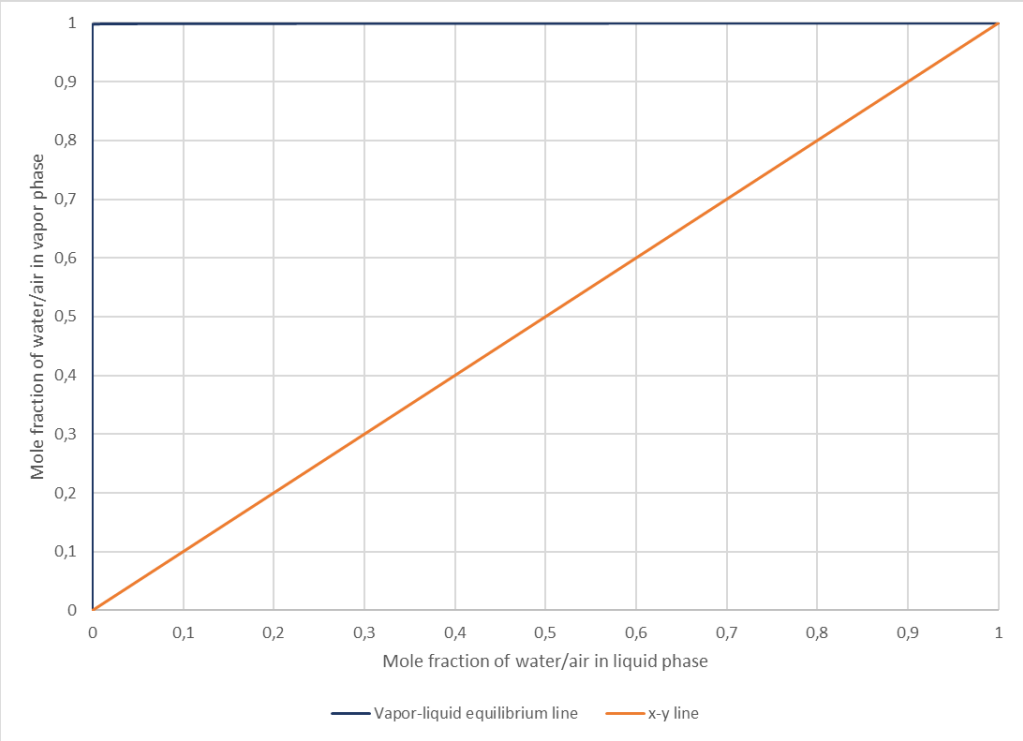

Figure 29: VLE diagram

4.3.2 Simulation

Table 7 shows the temperatures and mass flows of inputs and outputs of the RadFrac block. Air and water inputs are set values while outputs are calculated by Aspen Plus. As is evident from the output streams, the model is not running as intended. The actual water output at Chassix under these steady state conditions is 24 *°C*.

Additionally, the air flow out is not the same value as air flow in. In a cooling tower, all air flow that enters the tower exits through the output flow. Seeing that the input and output of air flow are not equal suggests the fact that the model does not run as expected.

Table 7: Stream results of the simulation

	Air in	**Air out**	**Water in**	**Water out**
Temperature [°C]	15	32.0361	32	31.9558

Mass flow [kg/hr]	217.51	105.354	62903.04	63015.20

Table 8 shows the values Quieros et al [3] got from their model in Aspen Plus. These values show how the RadFrac block in Aspen Plus has the ability to act as a Cooling tower, to the extent that the water is cooled down by the evaporation of water and not only as a heat exchanger. Comparing this to the values in this thesis it is clear that the model has some differences that does not enable it to act as a cooling tower.

Table 8: Flow values from article [3]

	Air in	**Water in**	**Water out**
Temperature [°C]	17.45	28.46	22.87

Temperature across all stages of the column is shown in Figure 30. The rate the temperature decreases is relatively constant from the first through fifth stages, where it drops drastically to the last stage. The drastic loss to the last stage is probably a result of air inlet and water outlet meeting there. Air is pulled in from the bottom of the column, stage 6, and exits at the top, on stage 1. Since water travels in the opposite direction through the tower, from 1 to 6, fresh air will meet water at the last stage. Because the air inlet is set to 15 *°C*, the temperature difference becomes much larger on this stage than on the rest. Vapor temperature across all the stages is listed in Table 9. These numbers show that the vapor temperature instantly assimilates to that of the liquid in the tower.

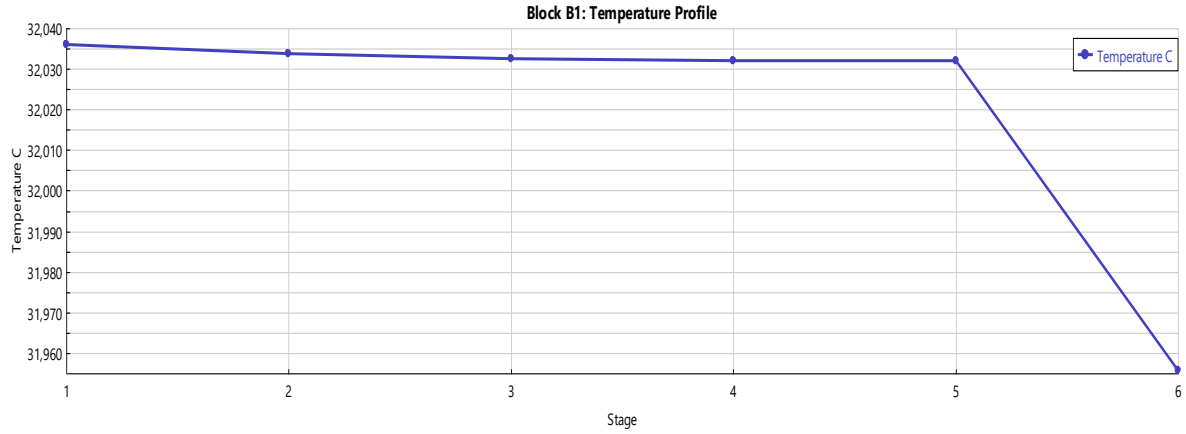

Figure 30: Temperature across stages

Table 9: Vapor and liquid temperature across stages

Stage	**Vapor temperature [°C]**	**Liquid temperature [°C]**
1	32.0337	32.0361
2	32.0326	32.0337

3	32.032	32.0326
4	32.0321	32.032
5	31.9558	32.0321
6	15	31.9558

Basic heat transfer calculations based on heat capacity shows that the liquid releases 5.648 *kW* over the last stage, while air absorbs 1.088 *kW*. This shows that the calculations of the model in Aspen Plus does not function even as a heat exchanger, much less a cooling tower. Figure 31 shows how the compositions remain constant throughout all stages, indicating that the model did not account for the evaporation of liquid in the column.

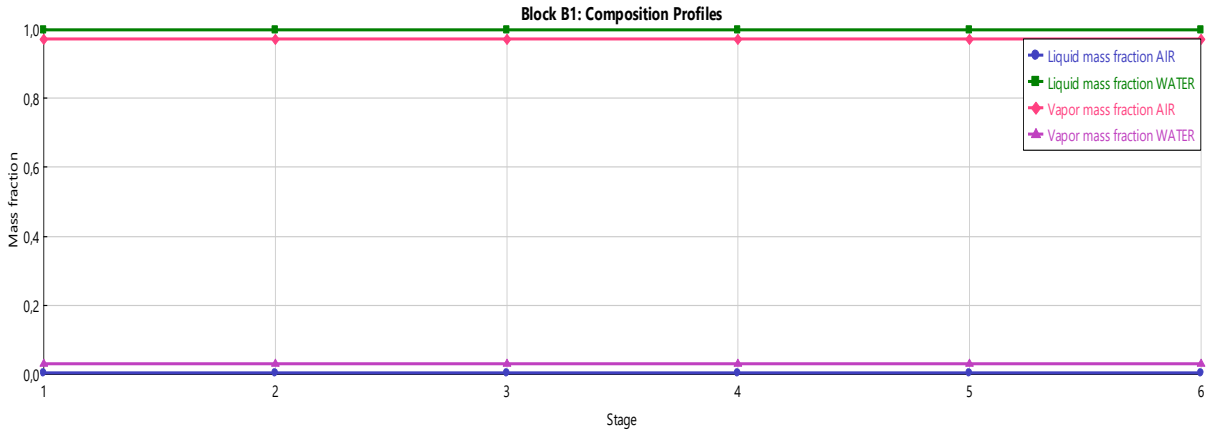

Figure 31: Composition of water and air across stages

5. Discussion

Both methods of calculating heat transfer were based on the initial insulation assumptions and subsequent heat transfer coefficients. These numbers were derived from the guesses at insulation composition. Fiber insulation has a much larger capacity for insulation, with its coefficient of 0.04 *W/m*K* compared to the coefficient for firebrick, 0.3 *W/m*K*. How much of the walls are made up of fiber insulation could greatly influence the resulting heat loss, but without knowing the accurate composition of the walls, this will be a significant uncertainty in the accuracy of the results.

Generalized heat transfer coefficients for convection varies from 6 to 30 W/m^2*K. When comparing this to the resulting coefficient calculated in this thesis, approximately 3 W/m^2*K for the tanks and 4 W/m^2*K for the chutes, this range would have been insufficient. This difference may arise from how the generalized coefficient range assumes that there is some natural draft. The tanks and chutes considered in this thesis are inside, without natural draft, which means that the only convective heat losses come from the movements created by the temperature difference. Because the temperature differences are in the area of only 25 – 40 *°C*, this likely causes such low coefficients.

The distribution of heat loss between tanks and chutes is fairly similar for calculations done both before and after measurements, with 4 % less for chutes and 4 % more for tanks in measurement calculations. The total heat loss, displayed in figure 25, shows that the heat loss from measurements is 36,65 % higher than calculations done before them. It is fair to assume that this number is the most accurate, since there were less assumed variables. Nevertheless, using thermal resistances to calculate heat loss without knowing surface temperature can provide answers that are in the same area as the actual heat loss, but will have a significantly higher degree of uncertainty.

Finding the Antoine constants for air was an uncertain process relying on several assumptions. Assuming that the vapor pressure of a gas is equal to the normal pressure is a thermodynamical assumption that is by no means supported or explored, but rather a leap of faith following the idea that the pressure naturally goes from one to the other when a liquid evaporates. An alternative could have been to use the ideal gas law to calculate the pressure in the gas state, but early calculations showed that the resulting numbers were not in accordance with tabulated values for the relevant temperature ranges.

Antoine constants for air were found for both boiling line and dew line. On the other hand, water was only represented by the Antoine constants valid from 0.01 *°C* to 373.98 *°C*. Using more sets of constants for other temperature ranges would have increased the accuracy of the VLE diagram that was produced.

The results from the simulation in Aspen Plus were not reasonable, and clearly showed that the internal mathematical models in the program did not produce the expected results. Of course, the model block, RadFrac, is intended for use as a distillation column, not a cooling tower. This shows that more experimentation in Aspen Plus was necessary before the model could be run successfully, operating as a cooling tower.

The difference in air flow input and output is significant, 112.15 *kg/hr*. One explanation could be that parts of the vapor in the air condenses in the RadFrac block, considering that the output of

water is higher than the input. However, the differences do not add up when comparing the amount of air that is missing, to the added water that exits the block.

Even though there was one earlier example of the RadFrac block functioning as a cooling tower, there are possibly several aspects of the model that needed to be adjusted for it to run in the intended manner, which were not uncovered during the work on this thesis. In hindsight, a program with built-in blocks and functions aimed at the operation of a cooling tower would have been easier to use if only an assessment of the operation was relevant.

In the future, solutions to the limitations encountered in this thesis could include: choosing a thesis with a well thought-out and specific problem and ensuring that the relevant company and contact persons have the opportunity to provide sufficient support.

6. Conclusion

Heat loss from the tanks and chutes at Chassix was estimated using two different methods, thermal resistance and calculated conductive, convective and radiative heat loss with surface temperature measurements. The method based on thermal resistance yielded a heat loss of 61.14 *kW* in total, which amounts to 605.65 *MWh* over one year. Calculations using the surface temperature produced a heat loss of 94.48 *kW*, which accumulates to 827.64 *MWh* over one year, 36.65 % more than the result without measurements. The results from surface temperature measurements are the most accurate because it is based on fewer assumptions.

A VLE diagram of air and water was created with the intention of using the McCabe-Thiele method to find the number of equilibrium stages in the cooling tower at Chassix. However, it was not reasonable to use the McCabe-Thiele method on the VLE diagram in this thesis. As an alternative, a reasonable number of equilibrium stages based on a published article was used.

A model of the cooling tower was created in Aspen Plus, using the RadFrac block, which represents a distillation column. After simulations, it was clear the model did not run as a cooling tower, nor did it produce any valid results.

Even if the work done in this thesis proved insufficient to simulate a cooling tower in Aspen Plus, it is not unreasonable that the model could function, but there needs to be a more explicit approach with a well explained method.

7. Recommendations

If it becomes relevant for Chassix to reduce the heat loss from the metal holding tanks and chutes, improving insulation would help. As the breakdown of insulation is assumed, the ratio of firebrick and fiber should first be checked. Because fiber has a much lower heat transfer coefficient, increasing the thickness of that layer would reduce heat loss. Having a surface material with lower emissivity would also reduce heat loss substantially, considering regular steel has more than 10 times lower emissivity than stainless steel.

Performing a successful energy analysis on a cooling tower using Aspen Plus has been performed before, with a different approach than in this thesis presented. More effort needs to be put towards creating a systematic and orderly method for Aspen Plus to be a feasible option when analyzing cooling tower performance.

8. List of References

1. Jin, G.-Y., et al., *A simplified modeling of mechanical cooling tower for control and optimization of HVAC systems.* Energy conversion and management, 2007. **48**(2): p. 355-365.
2. Stoecker, W.F., *Procedures for simulating the performance of components and systems for energy calculations*. 1975, American Society of Heating, Refrigerating, and Air-Conditioning Engineers, Inc., New York.
3. Queiroz, J.A., et al., *Modeling of existing cooling towers in ASPEN PLUS using an equilibrium stage method.* Energy conversion and management, 2012. **64**: p. 473-481.
4. Synne Krekling Lien, D.S., *Energibruk i Fastlands-Norge*, D. Spilde, Editor. 2017: Oslo.
5. Sørlie, J.-A., *Energy flow in a factory*. 2017, University of Agder: Grimstad.
6. Moran, S., Boettner, Bailey, *Principles of Engineering Thermodynamics*. 2012, Wiley. p. 4-5, 49-57, 147.
7. *Steady Heat Conduction*.
8. Kreith, M., Bohn, Tiwari, *Principles of heat transfer*. Seventh ed. 2003, Stamford, USA: Cengage Learning.
9. Mills, A.F., *Heat Transfer*. 1992, Boston. MA. 881.
10. *Emissivity Coefficients of some common Materials*. 2003 [cited 2018 22.05]; Available from: https://www.engineeringtoolbox.com/emissivity-coefficients-d_447.html.
11. T.Tham, M. *Distillation, an introduction*. 1997 2016 [cited 2018 21.03.2018]; Available from: http://www.rccostello.com/distil/distil0.htm
12. srsengineering. *How Columns Work?* 2016 [cited 2018 21.03.2018]; Available from: http://www.srsengineering.com/our-products/distillation-columns/how-columns-work/.
13. Duffy, G. *The McCabe Thiele*

Graphical Design

Method. [cited 2018 11.04.2018]; Available from: file:///C:/Users/jasoe/Downloads/McCabeThiele.pdf.

14. Price, R.M. *Distillation*. 1997 13.02.2003 [cited 2018 26.04]; Available from: http://facstaff.cbu.edu/rprice/lectures/distill.html.
15. Hensley, J.C., *Cooling tower fundamentals*. 1985: Marley Cooling Tower Company.
16. *How Cooling Towers Work (W/ Diagram, Pictures & Principles) 2017*. 2017, Cooling Tower Products.
17. Price, R.M. *Equilibrium Diagrams*. 2002 02.10.2003 [cited 2018 26.04]; Available from: http://facstaff.cbu.edu/rprice/lectures/equidiag.html.
18. Clark, J. *RAOULT'S LAW AND IDEAL MIXTURES OF LIQUIDS*. 2005 February 2014 [cited 2018 11.04.2018]; Available from: https://www.chemguide.co.uk/physical/phaseeqia/idealpd.html.
19. College, I.A.F. *Using VLE to Solve Material Balance Problems*. [cited 2018 12.04.2018]; Available from:

https://www.et.byu.edu/~rowley/ChEn273/Topics/Mass_Balances/Multiphase_Systems/Vapor_Liquid_Equilibrium/Data.htm.

20. Joshua Halpern, S.S., and Scott Johnson. *Vapor Pressure*. 2018 [cited 2018 12.04.2018]; Available from: https://chem.libretexts.org/Textbook_Maps/General_Chemistry_Textbook_Maps/Map%3A_Chemistry%3A_The_Central_Science_(Brown_et_al.)/11%3A_Liquids_and_Intermolecular_Forces/11.5%3A_Vapor_Pressure.

21. *CURVE FITTING DATA TO AN ANTOINE EQUATION*. 2015 09.08 [cited 2018 17.04]; Available from: https://cheguide.com/2015/08/curve-fitting-data-to-an-antoine-equation/.

22. J. D. Seader, E.J.H., *SEPARATION PROCESS PRINCIPLES*. second ed. 2006: John Wiley & Sons, Inc.

23. *Constant Molal Overflow (CMO)*. 2008 [cited 2018 27.04.2018]; Available from: http://pillars.che.pitt.edu/student/slide.cgi?course_id=12&slide_id=83.0.

24. Mazzotti, M. *Constant Molar Overflow (CMO) assumption*. [cited 2018 27.04]; Available from: http://www.hyper-tvt.ethz.ch/distillation-cmo.php.

25. BAF, E.a., J.-A. Sørlie, Editor. 2017.

26. Eden, M.R. *Introduction to Aspen Plus Simulation*. [cited 2018 03.04]; Available from: http://wp.auburn.edu/eden/wp-content/uploads/2012/03/4460-Aspen-Notes-2012.pdf.

27. Moran, S., Boettner, Bailey *Principles of Engineering Thermodynamics*. 2012: John Wiley & Sons.

28. Yaws, C.L., *The Yaws handbook of vapor pressure: Antoine coefficients*. 2015: Gulf Professional Publishing.

29. Shpilrain, E.E. *AIR (PROPERTIES OF)*. 2011 03.02.2011 [cited 2018 19.04]; Available from: http://www.thermopedia.com/content/553/.

30. contributors, W. *Bibliographic details for Introduction to Chemical Engineering Processes/Vapor-Liquid equilibrium*. 2017 10.11 [cited 2018 23.04]; Available from: https://en.wikibooks.org/w/index.php?title=Introduction_to_Chemical_Engineering_Processes/Vapor-Liquid_equilibrium&oldid=3325807.

9. Appendices

9.2 Heat loss calculations for tanks

Rayleigh	Ambient temp	Surface temp	Reference temp	surf temp ©	Beta	Nu function	Nusselt	h coefficient	Convection	Radiation	Conduction	Total
13943085923	293,15	323,15	308,15	50	0,00324517	0,34260194	176,821619	2,77179836	4,14904952	7,965891488	17,172909	29,28785
16136023118	293,15	328,15	310,65	55	0,00321906	0,34260194	183,37278	2,87449223	5,01989826	9,529210519	17,0466098	31,5957186
18293946148	293,15	333,15	313,15	60	0,00319336	0,34260194	189,196387	2,9657812	5,91922475	11,1656471	16,9203105	34,0051824
20417686966	293,15	338,15	315,65	65	0,00316807	0,34260194	194,444358	3,04804669	6,8438402	12,87744631	16,7940113	36,5152978
22508051376	293,15	343,15	318,15	70	0,00314317	0,34260194	199,223984	3,12297057	7,79118697	14,66688714	16,667712	39,1257861
24565820052	293,15	348,15	320,65	75	0,00311867	0,34260194	203,614121	3,19178893	8,75916252	16,53628256	16,5414128	41,8368578
26591749510	293,15	353,15	323,15	80	0,00309454	0,34260194	207,674586	3,25543946	9,74600442	18,48797948	16,4151135	44,6490974
28586573035	293,15	358,15	325,65	85	0,00307078	0,34260194	211,451935	3,31465195	10,7502118	20,52435877	16,2888143	47,5633848
30551001564	293,15	363,15	328,15	90	0,00304739	0,34260194	214,983183	3,37000665	11,7704896	22,64783522	16,162515	50,5808399
32485724536	293,15	368,15	330,65	95	0,00302435	0,34260194	218,298292	3,42197323	12,8057082	24,86085761	16,0362158	53,7027816
34391410693	293,15	373,15	333,15	100	0,00300165	0,34260194	221,42189	3,47093773	13,8548727	27,16590863	15,9099165	56,9306979
36268708854	293,15	378,15	335,65	105	0,00297929	0,34260194	224,374488	3,5172217	14,9171	29,56550495	15,7836173	60,2662222
38118248651	293,15	383,15	338,15	110	0,00295727	0,34260194	227,17337	3,56109607	15,9916004	32,06219717	15,657318	63,7111156
39940641233	293,15	388,15	340,65	115	0,00293556	0,34260194	229,833248	3,60279145	17,0776638	34,65856985	15,5310188	67,2672524
41736479937	293,15	393,15	343,15	120	0,00291418	0,34260194	232,366758	3,64250594	18,1746476	37,35724148	15,4047195	70,9366087
43506340937	293,15	398,15	345,65	125	0,0028931	0,34260194	234,784843	3,68041105	19,2819679	40,16086454	15,2784203	74,7212528

9.3 Heat loss calculations for chutes

Rayleigh	Surface temp	Ref temp	Surf temp ©	Beta	Nusselt	H coefficient	Convection	Radiation	Conduction	Total
70856975,7	313,15	303,15	40	0,0032987	47,7092347	3,82083776	4,86927564	6,44887315	50,6973524	62,0155012
87846769,9	318,15	305,65	45	0,00327172	50,3053643	4,02875118	6,41780062	8,26699686	50,3299004	65,0146979
104560890	323,15	308,15	50	0,00324517	52,5139824	4,20563038	8,03948303	10,1728917	49,9624484	68,1748232
121005992	328,15	310,65	55	0,00321906	54,4418219	4,36002317	9,72372367	12,1693381	49,5949964	71,4880582
137188518	333,15	313,15	60	0,00319336	56,1555606	4,49726951	11,4626405	14,2591597	49,2275444	74,9493447
153114707	338,15	315,65	65	0,00316807	57,6999045	4,6209497	13,2501112	16,4452236	48,8600924	78,5554273
168790603	343,15	318,15	70	0,00314317	59,1064266	4,73359231	15,0812251	18,7304403	48,4926404	82,3043058
184222060	348,15	320,65	75	0,00311867	60,3983318	4,83705572	16,9519455	21,1177634	48,1251884	86,1948974
199414750	353,15	323,15	80	0,00309454	61,5932229	4,93274967	18,8588885	23,6101902	47,7577364	90,2268152
214374174	358,15	325,65	85	0,00307078	62,7048003	5,02177136	20,7991726	26,2107612	47,3902844	94,4002183
229105661	363,15	328,15	90	0,00304739	63,7439565	5,10499314	22,7703114	28,9225601	47,0228324	98,715704
243614383	368,15	330,65	95	0,00302435	64,7195085	5,18312112	24,7701358	31,7487143	46,6553804	103,174231
257905354	373,15	333,15	100	0,00300165	65,6387035	5,25673569	26,7967358	34,6923941	46,2879284	107,777058
271983440	378,15	335,65	105	0,00297929	66,5075777	5,32632028	28,8484159	37,7568137	45,9204764	112,525706
285853363	383,15	338,15	110	0,00295727	67,3312172	5,3922822	30,92366	40,9452302	45,5530244	117,421915
299519706	388,15	340,65	115	0,00293556	68,1139514	5,45496819	33,0211044	44,2609442	45,1855724	122,467621

9.4 Antoine constants for air along boiling line

Air(boiling)			
Temperature	Pressure	T(estimert)	T(diff)
-208,15	0,1468	-208,22131	0,00508465
-203,15	0,3234	-203,12101	0,00084061
-193,15	1,146	-193,05929	0,0082276
-183,15	3,036	-183,11433	0,00127252
-173,15	6,621	-173,19457	0,00198626
-163,15	12,59	-163,22287	0,00531032
-153,15	21,61	-153,16978	0,00039128
-143,15	34,16	-143,09679	0,00283088
Antoine Constants		Sum T(diff)	0,02594413
A	3,91289728		
B	310,735972		
C	273,692179		

9.5 Antoine constants for air along condensing line

Air(condensing)			
Temperature	Pressure	T(estimert)	T(diff)
-208,15	0,08613	-208,20738	0,00329292
-203,15	0,2052	-203,12581	0,00058537
-193,15	0,8245	-193,05808	0,00844959
-183,15	2,397	-183,09289	0,00326101
-173,15	5,599	-173,18195	0,00102095
-163,15	11,22	-163,25383	0,01078014
-153,15	20,14	-153,21351	0,00403337
-143,15	33,2	-143,04378	0,0112829
Antoine Constants		Sum T(diff)	0,04270624
A	4,06134455		
B	328,127822		
C	272,217461		